



## Drivers of Marine CO<sub>2</sub>-Carbonate Chemistry in the Northern Antarctic Peninsula

Maurício Santos-andrade, Rodrigo Kerr, Iole B M Orselli, Thiago Monteiro, Mauricio M Mata, Catherine Goyet

### ► To cite this version:

Maurício Santos-andrade, Rodrigo Kerr, Iole B M Orselli, Thiago Monteiro, Mauricio M Mata, et al.. Drivers of Marine CO<sub>2</sub>-Carbonate Chemistry in the Northern Antarctic Peninsula. Global Biogeochemical Cycles, 2023, 37 (3), 10.1029/2022GB007518 . hal-04050313

**HAL Id: hal-04050313**

**<https://univ-perp.hal.science/hal-04050313>**

Submitted on 29 Mar 2023

**HAL** is a multi-disciplinary open access archive for the deposit and dissemination of scientific research documents, whether they are published or not. The documents may come from teaching and research institutions in France or abroad, or from public or private research centers.

L'archive ouverte pluridisciplinaire **HAL**, est destinée au dépôt et à la diffusion de documents scientifiques de niveau recherche, publiés ou non, émanant des établissements d'enseignement et de recherche français ou étrangers, des laboratoires publics ou privés.

# Global Biogeochemical Cycles®

## RESEARCH ARTICLE

10.1029/2022GB007518

### Key Points:

- The western basin experiences steeper pH decreases than the surrounding areas at a rate of  $-0.017 \text{ pH}_{\text{sw}} \text{ units yr}^{-1}$  due to Circumpolar Deep Water intrusions
- Dense Shelf Water inflow into the deep layer of the central basin promoted a CT increase of about  $50 \mu\text{mol kg}^{-1}$  in the 2010s relative to the 2000s
- Internal mixing has likely reduced spatiotemporal variability of carbonate chemistry in the eastern basin since the 1990s

### Supporting Information:

Supporting Information may be found in the online version of this article.

### Correspondence to:

M. Santos-Andrade and R. Kerr,  
[mauricios@furg.br](mailto:mauricios@furg.br);  
[rodrigokerr@furg.br](mailto:rodrigokerr@furg.br)

### Citation:

Santos-Andrade, M., Kerr, R., Orselli, I. B. M., Monteiro, T., Mata, M. M., & Goyet, C. (2023). Drivers of marine  $\text{CO}_2$ -carbonate chemistry in the northern Antarctic Peninsula. *Global Biogeochemical Cycles*, 37, e2022GB007518. <https://doi.org/10.1029/2022GB007518>







Received 7 JUL 2022

Accepted 16 FEB 2023

### Author Contributions:

**Conceptualization:** Maurício Santos-Andrade, Rodrigo Kerr  
**Data curation:** Maurício Santos-Andrade  
**Formal analysis:** Maurício Santos-Andrade  
**Funding acquisition:** Rodrigo Kerr, Maurício M. Mata  
**Investigation:** Maurício Santos-Andrade, Rodrigo Kerr  
**Supervision:** Rodrigo Kerr  
**Validation:** Maurício Santos-Andrade  
**Writing – original draft:** Maurício Santos-Andrade, Rodrigo Kerr  
**Writing – review & editing:** Iole B. M. Orselli, Thiago Monteiro, Maurício M. Mata, Catherine Goyet

## Drivers of Marine $\text{CO}_2$ -Carbonate Chemistry in the Northern Antarctic Peninsula

Maurício Santos-Andrade<sup>1,2</sup> , Rodrigo Kerr<sup>1,2</sup> , Iole B. M. Orselli<sup>1,2</sup> , Thiago Monteiro<sup>1,2</sup> ,  
Mauricio M. Mata<sup>1,2</sup> , and Catherine Goyet<sup>3,4</sup> 

<sup>1</sup>Laboratório de Estudos dos Oceanos e Clima, Instituto de Oceanografia, Universidade Federal do Rio Grande – FURG, Rio Grande, Brazil, <sup>2</sup>Programa de Pós-Graduação em Oceanologia, Instituto de Oceanografia, Universidade Federal do Rio Grande – FURG, Rio Grande, Brazil, <sup>3</sup>ESPACE-DEV, Université de Perpignan Via Domitia, Perpignan, France, <sup>4</sup>ESPACE-DEV UMR, Université de Perpignan Via Domitia, IRD, Montpellier, France

**Abstract** The Bransfield Strait is a climate change hotspot at the tip of the northern Antarctic Peninsula (NAP). The region is marked by a mixture of relatively warm waters from the Bellingshausen Sea with cold shelf waters from the Weddell Sea. Additionally, its deep central basin ( $>800 \text{ m}$ ) preserves seawater properties from the north-western Weddell Sea continental shelf. This study assessed long-term changes in carbonate chemistry in the Bransfield Strait and found that the hydrographic setting (i.e., a mixture between modified-Circumpolar Deep Water with Dense Shelf Water [DSW]) drives temporal variability of carbonate parameters. The western basin has experienced decreases in pH (seawater scale) over the last three decades (1996–2019), varying from  $-0.003$  to  $-0.017 \text{ pH units yr}^{-1}$ , while  $\Omega_{\text{ar}}$  decreased from  $-0.01$  to  $-0.07 \text{ yr}^{-1}$  throughout the water column. The central basin was characterized by a high contribution of DSW with high carbon dioxide ( $\text{CO}_2$ ) content and the decomposition of organic matter produced and transported into its deep layer. With lower variability for all carbonate system variables, the eastern basin was likely regulated by internal mixing. Overall, the entire strait is almost reaching a  $\text{CO}_2$ -saturated condition, highlighting how sensitive subpolar regions are to the effects of human-induced climate change.

**Plain Language Summary** Although the entire world is experiencing the impacts of climate change, they may be occurring more rapidly in some regions, such as the northern Antarctic Peninsula. At the northern tip of this area is the Bransfield Strait, which can act as a sentinel for identifying what is happening around the peninsula during modern climate change. Areas of the strait that are connected to the open ocean showed a more rapid increase in acidification over time than areas mainly influenced by coastal zones. This occurs because the contribution of open-ocean water masses supplies a signature of the decomposition of organic particles from the ocean around Antarctica. On the other hand, coastal zones are more influenced by atmospheric carbon dioxide from human activities. The steeper acidification trends in the Bransfield Strait draw our attention to the effects of climate change on ocean acidification and its biological and chemical impacts on the ocean. Moreover, there are many areas, such as the Bransfield Strait, for which there are few studies about these effects, which delays the identification of severe impacts even after changes have already been experienced, as was found in our assessment.

## 1. Introduction

In the next few decades, the Southern Ocean is expected to become the next oceanic region, after the Arctic Ocean, to experience a subsaturated aragonite condition throughout the water column (Henley et al., 2020; Orr et al., 2005). There is an indication that calcium carbonate dissolution will prevail over precipitation, affecting unstable (aragonite) and stable (calcite) biogenic calcium carbonate minerals formed by different marine organisms. Moreover, many other climate-driven impacts have been observed around the Antarctic continent, including (a) an increase in atmospheric and ocean surface temperatures (Cook et al., 2005; Meredith & King, 2005; Siebert et al., 2019); (b) intensification of westerly winds related to modes of climate variability and their impacts surrounding Antarctica (Turner et al., 2007); and (c) glacial retraction and changes in the concentration, duration, and extension of sea ice (Cook et al., 2016; Rignot et al., 2019). Concomitantly, hydrographic and biogeochemical changes in ocean water masses are taking place around Antarctica, such as freshening trends of shelf and deep waters (Azaneu et al., 2013; De Lavergne et al., 2014; Dotto et al., 2016; Haumann et al., 2016; Hellmer et al., 2011), increased frequency of Circumpolar Deep Water (CDW) intrusions into coastal environments (Henley

et al., 2019; Moffat & Meredith, 2018) and pH reduction over different time scales (McNeil & Matear, 2008; Midorikawa et al., 2012; Roden et al., 2013; Sabine et al., 2008). These changes are already impacting and changing the behavior of Southern Ocean ecosystems, which impact ocean health for the development of the sensitive Antarctic biota with different environmental roles, such as biogeochemical recycling and vertical energy fluxes (Figuerola et al., 2020, 2021; Henley et al., 2020; Mendes et al., 2023).

In this sense, Southern Ocean coastal zones, such as the northern Antarctic Peninsula (NAP), are more sensitive to the effects of climate change (Kerr, Mata, et al., 2018). The surrounding waters of the NAP have experienced (a) an increase in partial pressure of carbon dioxide ( $p\text{CO}_2$ ) in deep waters, as also observed in the Weddell Sea (van Heuven et al., 2014); (b) glacier retraction and changes in sea ice thickness over recent decades, such as for the Larsen ice shelves (Cook et al., 2005, 2016; Dinniman et al., 2011, 2012); and (c) impacts of modes of climate variability altering hydrographic patterns in the region, such as the frequency and intensity of water masses coming from open ocean regions (Ruiz Barlett et al., 2018). Other biogeochemical impacts have been highlighted around the NAP, such as the increased anthropogenic carbon observed in recently ventilated waters (Kerr, Goyet, et al., 2018) and its effect on decreasing pH along the NAP (Lencina-Avila et al., 2018), in addition to increasing carbon dioxide ( $\text{CO}_2$ ) uptake during summers since 2012 in coastal zones (Monteiro, Kerr, Orselli, et al., 2020).

However, our understanding of carbonate chemistry in the Bransfield Strait is minimal. Current knowledge is limited to regional (e.g., the FRUELA cruise in 1996 in the western basin of the Bransfield Strait) and temporal (either only 1 year of summer data or short-time series) assessments (e.g., Anadón & Estrada, 2002; Ito et al., 2018). Nevertheless, many efforts to comprehend the carbonate system along the NAP over recent decades (Orselli et al., 2022 and references therein) have focused on southern regions of the western Antarctic Peninsula (Kerr, Goyet, et al., 2018; Kerr, Orselli, et al., 2018; Legge et al., 2017; Lencina-Avila et al., 2018; Monteiro, Kerr, & Machado, 2020; Monteiro, Kerr, Orselli, et al., 2020; Rivaro et al., 2014; Sandrini et al., 2007).

Some characteristics of the Bransfield Strait pinpoint particular interest in unraveling the variability of carbonate chemistry. Besides acting as a transitional environment between polar and subpolar domains, the NAP region interconnects the warm and old intermediate waters derived from the Bellingshausen Sea with the cold and young waters sourced in the Weddell Sea continental shelf (Ruiz Barlett et al., 2018; van Caspel et al., 2018). Furthermore, the Bransfield Strait is considered a sentinel for preserving and tracking both hydrographic and biogeochemical processes around the NAP, as its deep layers maintain seawater properties of the shelf waters sourced in the Weddell Sea (Azaneu et al., 2013; Dotto et al., 2016; Gordon et al., 2000; Hofmann et al., 1996).

Considering the key role of the Bransfield Strait in connecting environments along the NAP, we evaluated for the first time the spatial and temporal variability of carbonate system parameters (i.e., total alkalinity [TA], total inorganic carbon [CT],  $p\text{CO}_2$ , pH, and the saturation state of aragonite and calcite carbonate minerals— $\Omega_{\text{ar}}$  and  $\Omega_{\text{ca}}$ , respectively) in a period spanning 30 years during 1990–2019. We used hydrographic and biogeochemical data available in historical (World Ocean Database 2018—WOD18, 1996, 2006, and 2010) and recent (Brazilian High Latitude Oceanography Group—GOAL, 2015–2019) databases to estimate equations able to reconstruct carbonate system parameters in the three basins of the Bransfield Strait over the last three decades (i.e., 1990s, 2000s, and 2010s). The results presented here will lead to a better understanding of the main drivers of interannual variability, as well as decadal changes, of carbonate chemistry in the study area.

## 2. Oceanographic Features of the Bransfield Strait

### 2.1. Geomorphological Setting of the Bransfield Strait

The Bransfield Strait (Figure 1a) is a coastal area of the NAP consisting of three deep basins formed by a rifting system that splits the South Shetland Islands from the Antarctic Peninsula, leading to a heritage of some volcanoes and fault systems in the region (Fisk, 1990). The release of hydrothermal fluids and magma in deep and shallow waters has recently been identified, as is the case for the Humpback volcano (Almendros et al., 2020) and Deception Island (Álvarez-Valero et al., 2020), respectively.

The depth of the Bransfield Strait increases from the southwest toward the northeast, from ~1,200 m in the western basin, reaching ~2,000 m in the central basin and then a maximum of ~2,500 m in the eastern basin. All deep basins are bound by deep canyons and sills shallower than 800 m (Clowes, 1934; Lopez et al., 1999; Masqué et al., 2002). While the western basin has an open connection to the Bellingshausen Sea, the others are semiclosed systems with much more influence from the continental shelf of the Weddell Sea.

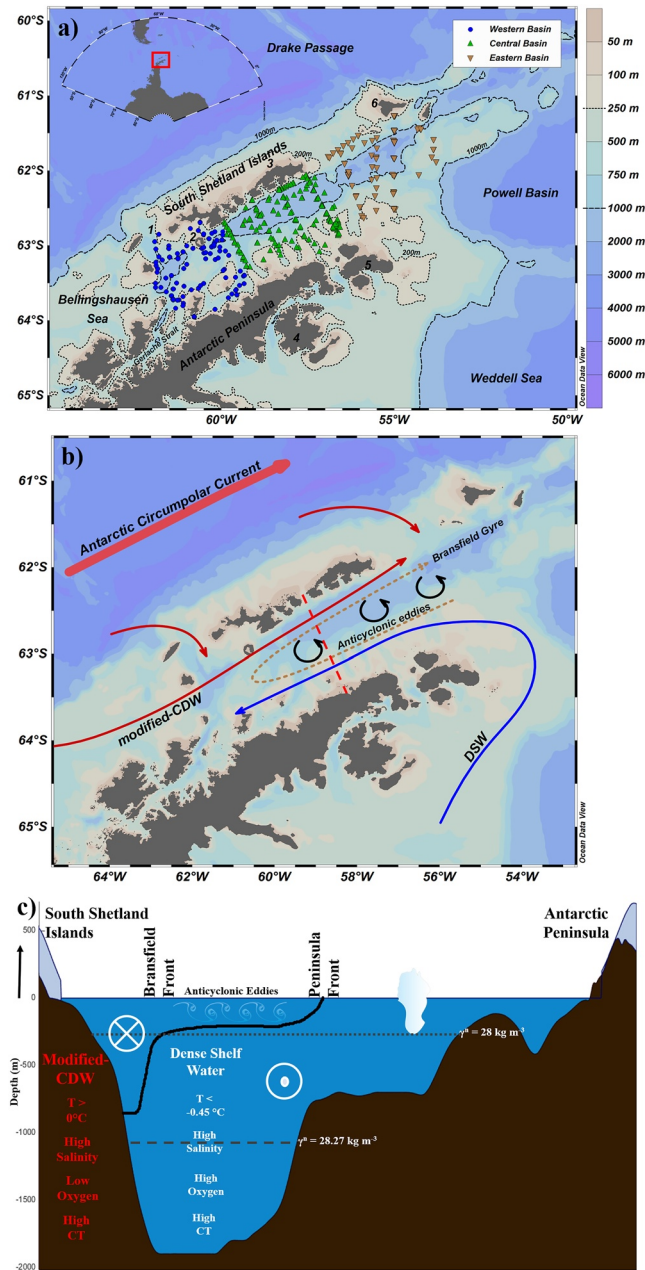


**Figure 1.** The Bransfield Strait and its main characteristics. (a) Distribution of the oceanographic stations used in this study. Stations in the western, central, and eastern basins of the Bransfield Strait are marked by blue dots, green triangles, and brown inverted triangles, respectively. The black dashed line shows the 1,000 m isobath, while the black dotted line shows the 200 m isobath. The numbers indicate the following: 1. Boyd Strait, 2. Deception Island, 3. King George Island, 4. James Ross Island, 5. Joinville Island, and 6. Clarence Island. (b) Ocean circulation scheme around the northern Antarctic Peninsula. Red arrows indicate the pathways of modified Circumpolar Deep Water (modified-Circumpolar Deep Water [CDW]), while the blue arrow indicates the pathway of Dense Shelf Water (DSW). The boundary between modified-CDW and DSW triggers anticyclonic eddies in the cyclonic Bransfield Gyre. The red dashed line indicates the section described in panel (c). (c) Scheme of the main hydrographic properties (seawater temperature— $T$  and total inorganic carbon— $CT$ ) and ocean dynamics along the red dashed line depicted in panel (b). The in and out arrows represent the direction of the main current flow in the region, which is northward around the South Shetland Islands and southward near the Antarctic Peninsula. The dotted and dashed lines indicate the mean depth related to neutral density ( $\gamma^n = 28$  and  $\gamma^n = 28.27 \text{ kg m}^{-3}$ , respectively). The black line represents the boundary between modified-CDW and DSW.

## 2.2. Hydrographic Dynamics of the Bransfield Strait

The main water mass contribution influencing the intermediate levels of the Bransfield Strait is advected from the Bellingshausen Sea and the Drake Passage, with relatively warm temperatures, hereinafter referred to as modified-CDW (Figure 1b). It is derived from a mixture of surface waters and CDW intrusions over the continental shelf of the western Antarctic Peninsula (Huneke et al., 2016; Moffat & Meredith, 2018; Sangrà et al., 2011). Intense modified-CDW intrusions are usually related to stronger westerlies during periods of Southern Annular Mode (SAM) in positive phases (SAM+), El-Niño Southern Oscillation (ENSO) in negative phases (ENSO−) or their coupled events (Loeb et al., 2009; Ruiz Barlett et al., 2018). For instance, Ruiz Barlett et al. (2018) pointed out that the early 2000s, characterized by joint events of SAM+ and ENSO−, presented a hydrographic setting favored by modified-CDW intrusions into the western basin of the Bransfield Strait between 500 and 800 m in depth, corresponding to 80% of the water mass structure.

In addition, the deep basins of the Bransfield Strait are filled with Dense Shelf Water (DSW) advected from the north-western and southern continental shelf of the Weddell Sea and characterized by high density and low temperatures close to the freezing point of seawater (Figure 1b, Frölicher et al., 2015; Hellmer et al., 2017; Sangrà et al., 2011, 2017). Thus, the DSW considered here does not account for the differentiation between High Salinity Shelf Water and Low Salinity Shelf Water sourced by ocean-atmosphere-sea ice interactions in the north-western continental shelves (e.g., Damini et al., 2022; Dotto et al., 2016) and Ice Shelf Water derived from ocean-ice shelf processes in the southern continental shelves (Nicholls et al., 2009). The influence of Ice Shelf Water on the composition of DSW in the deep layers of the Bransfield Strait is still a challenge (e.g., Damini et al., 2022; van Caspel et al., 2018; Wang et al., 2022), but an overflow is expected in the vicinity of the Powell Basin into the eastern basin (Gordon et al., 2000; Von Gyldenfeldt et al., 2002). A larger contribution of DSW in the Bransfield Strait occurs during weaker westerlies, events of SAM− and ENSO+ or joint events of both phases (Ruiz Barlett et al., 2018), which intensify the Weddell Gyre. An intensification of DSW was identified during the 2010s, representing at least 60% of the water mass structure in the deep layer of the central basin (Damini et al., 2022).

The averaged water mass fractions of contribution in the western, central and eastern basins of Bransfield Strait, excluding the surface level up to ~100 m, are 80%, 40%, and 60% of CDW plus 20%, 60%, and 40% of DSW, respectively (Figure S1 in Supporting Information S1). However, a high degree of interannual variability in the water mass fractions is expected due to the rapid replenishment of DSW and CDW intrusions in the region (Damini et al., 2022; Dotto et al., 2016).

The boundary between the modified-CDW and DSW is associated with the surface Peninsula Front and the subsurface Bransfield Front (Figure 1c, Sangrà et al., 2011, 2017). The circulation pattern of both water masses in the strait characterizes a cyclonic gyre, the Bransfield Gyre (Moffat & Meredith, 2018), with intense baroclinic jets to the northeast associated with the Bransfield Current in the Bransfield Front (Sangrà et al., 2011, 2017). This current plays a crucial role in toting metal, nutrients, and organisms along the Bransfield Strait (Zhou et al., 2006). Furthermore, another reason for the complex hydrography is related to glacier and sea ice melting around Antarctica (Castro et al., 2002), including the western Weddell Sea with the collapse of Larsen ice shelves (Massom et al., 2018; Scambos et al., 2000) and coastal ice coverage of the western Antarctic Peninsula, which is influenced by the heat transport of CDW (Meredith et al., 2008, 2014; Shepherd et al., 2004, 2018). For a broad review of the hydrography of the Bransfield Strait, the reader should refer to Clowes (1934), Damini et al. (2022), Dotto et al. (2016), García et al. (2002), Sangrà et al. (2011, 2017), and Ruiz Barlett et al. (2018).

## 2.3. Biogeochemical Aspects of the Bransfield Strait

The coastal zones along the NAP are areas of high biological productivity during summers, holding high stocks and concentrations of phytoplankton (Karl et al., 1990; Mendes et al., 2012), with diatoms being the most abundant phytoplanktonic group found in the north-western Weddell Sea (Mendes et al., 2012). This, therefore, implies high organic matter sedimentation around the entire peninsula (Fischer, 1991; Masqué et al., 2002). Also, intense primary production in the north-western Weddell Sea continental shelf (Detoni et al., 2015; Mendes et al., 2012) likely promotes high dissolved organic carbon concentrations in the deep basins of Bransfield Strait (Avelina et al., 2020). Furthermore, regions related to islands and coastal zones in the strait are also associated with high organic carbon concentrations, such as Deception Island and Admiralty Bay (Costa et al., 2022; Doval et al., 2002).



The inorganic carbon cycle of the Bransfield Strait experiences large interannual variability, swinging between periods of net CO<sub>2</sub> source to the atmosphere (2009) and net CO<sub>2</sub> sink toward the ocean (2008 and 2010, Ito et al., 2018). This behavior has been recently pointed to be influenced by the strength of mesoscale structures, such as anticyclonic eddies (e.g., Damini et al., 2023). A long-term assessment of CO<sub>2</sub> fluxes in the vicinity of the Bransfield Strait has shown that coastal zones have acted as strong CO<sub>2</sub> sink zones since 2012 (Monteiro, Kerr, Orselli, et al., 2020), which is also observed southwards (Brown et al., 2019). The region has also stored ~20–50 μmol kg<sup>-1</sup> of anthropogenic carbon around the NAP (Anderson et al., 1991; Lencina-Avila et al., 2018; Pardo et al., 2014), which likely comes from recently ventilated DSW (Kerr, Goyet, et al., 2018). Moreover, some recent studies have also shown the impacts of ENSO or SAM on physical, biological, and biogeochemical parameters in the strait (Avelina et al., 2020; Costa et al., 2020; Damini et al., 2022; Dotto et al., 2016). A recent overview of state-of-the-art of carbonate chemistry and the challenges facing the NAP environments can be viewed in Orselli et al. (2022) and references therein.

### 3. Methods

#### 3.1. Data Collection

The following seawater hydrographic and biogeochemical variables were accessed from two data sets with broad coverage for austral summer (January, February, and March) in the Bransfield Strait: temperature (°C), salinity (unitless), dissolved oxygen as O<sub>2</sub> (μmol kg<sup>-1</sup>), TA (μmol kg<sup>-1</sup>), and CT (μmol kg<sup>-1</sup>). The compiled database used here is described below:

1. WOD18: A data set created by the National Centers for Environmental Information/National Oceanic and Atmospheric Administration with an associated high level of quality control. It includes hydrographic and biogeochemical data for different ocean regions spanning a long period of time (Boyer et al., 2018). The hydrographic variables were selected from ocean station data and high-resolution CDT/XCTD (<https://www.nodc.noaa.gov/OC5/WOD/wod18-notes.html>, Boyer et al., 2018) during 1990–2011. The precision for temperature and practical salinity measurements are 0.001°C–0.005°C and 0.003°C–0.02°C, respectively (Boyer et al., 2018). In situ TA and CT measurements were available for 1996, 2006, and 2010. For the FRUELA cruise (17 January–5 February 1996, Anadón & Estrada, 2002), TA and CT were determined through automatic potentiometric titration with hydrochloric acid and thermodynamic equations of the carbonate system estimated from pH at 15°C and TA (Alvarez et al., 2002). Neither quality control nor precision of in situ measurements was found for 2006 and 2010 data. The oceanographic stations containing TA and CT data available in WOD18 are presented in Figure S2a in Supporting Information S1.
2. GOAL: The GOAL data set included cruises in the NAP region, almost every year, comprising data of Bransfield and Gerlache straits, Drake Passage, and Bellingshausen and Weddell seas (Dotto, Mata, et al., 2021; Mata et al., 2018). The hydrographic data set is available at PANGAEA (Mata & Garcia, 2016a, 2016b, 2016c, 2016d, 2016e, 2016f; Mata & Kerr, 2016a, 2016b, 2016c) and NAPv.1. climatology at <https://doi.org/10.5281/zenodo.4420006> (Dotto, Kerr, et al., 2021), spanning from 2003 to 2019. During austral summers, the GOAL data set includes 58028 measurements for temperature and salinity against 28725 measurements for O<sub>2</sub>. The precision for temperature and practical salinity measurements are ~0.001°C and ~0.003°C, respectively (Dotto, Kerr, et al., 2021). The TA and CT measurements spanned 2015–2019 (Orselli et al., 2022) and were measured simultaneously by potentiometric titration in a closed cell with an automated titrator (see details at Kerr, Orselli et al. (2018); Figure S2b in Supporting Information S1). Quality control of TA and CT data was performed through analyses of Certified Reference Material from the Scripps Institution of Oceanography (Dickson et al., 2003). The average precisions for TA and CT were 3.2 ± 1.3 and 4.0 ± 0.8 μmol kg<sup>-1</sup>, respectively (Table S1 in Supporting Information S1). The precision was evaluated daily throughout the analysis period with replicate analysis of a single sample.

Since the hydrographic data from WOD18 and GOAL had already undergone serious quality control, only data marked with good quality by the postprocessing procedure in the data set (flag = 0 or 1) were used in this study (Boyer et al., 2018). The WOD18 and GOAL biogeochemical data sets (i.e., TA and CT) were also checked to identify potential spurious data since no quality control was previously described for either. Spurious data were excluded when greater than two standard deviations from the mean property value of each vertical profile. This represents only 3% and 8% of data for both TA and CT in WOD18 and GOAL, respectively. Validation of biogeochemical data was performed through comparisons with recently published climatologies (Broullón

et al., 2019, 2020). Finally, the database used here (WOD18 + GOAL) covers 30 years (1990–2019) for hydrographic and 23 years (1996–2019) for biogeochemical variables. The TA and CT variables available in WOD18 and GOAL were used to reconstruct the carbonate chemistry in the study area for the whole period through the hydrographic data (see Section 3.3). The spatial distribution and the number of occupations of each station with hydrographic data over the last three decades are presented in Figure S2c in Supporting Information S1.

### 3.2. Hydrographic-Derived Parameters

Neutral density ( $\gamma^n$ , kg m<sup>-3</sup>) and potential temperature ( $\theta$ , °C) were estimated according to EOS-80 (Fofonoff & Millard, 1983). The  $\gamma^n$  values were used to split the vertical layer structure in each basin (marked by their boundaries with sills shallower than 800 m, Figure 1b, Clowes, 1934; G rcia et al., 2002), defining the surface ( $\gamma^n \leq 28.00$  kg m<sup>-3</sup>), intermediate ( $28.00 < \gamma^n < 28.27$  kg m<sup>-3</sup>), and deep ( $\gamma^n \geq 28.27$  kg m<sup>-3</sup>) layers. The surface layer is occupied by Antarctic Surface Water that is highly modified locally by sea-air interactions, sea ice melting and continental meltwater inputs (Hofmann et al., 1996; Wang et al., 2022), whereas the intermediate layer is mainly composed of a mixture of modified-CDW and DSW (Ruiz Barlett et al., 2018; Wang et al., 2022). The deep layer is occupied by DSW that flows down the hills and canyons in the region (e.g., Dotto et al., 2016; Huneke et al., 2016; Ruiz Barlett et al., 2018; van Caspel et al., 2018).

### 3.3. Reconstruction of Marine Carbonate Chemistry

Since measured TA and CT data were not available for the entire period of study, we applied multivariate linear equations to reconstruct TA and CT over time in vertical profiles of the Bransfield Strait. This method allows the characterization of the variability of carbonate chemistry with respect to water masses and their hydrographic signatures since (a) TA is controlled by salinity changes through freshwater input or removal, which also impacts CT; (b) blooms of primary producers and their decomposition follow temperature changes (higher temperatures in the surface layer and lower throughout the depth), contribution to CT changes and a minor impact to TA changes; and (c) CO<sub>2</sub> ingassing is associated with the surface layer and its lower temperatures, which promotes CT changes and no impact on TA (Lee et al., 2006; Millero et al., 1998). Dissolved oxygen (O<sub>2</sub>) fits as a good proxy for biological processes and since they exhibit much more pronounced impacts on CT than TA, is added to CT reconstructions (Goyet & Davis, 1997).

This approach has been widely applied in different ocean regions, from global (Bittig et al., 2018; Carter et al., 2018) to regional (Arrigo et al., 2010; Orselli et al., 2019) scales, including along the NAP (Hauri et al., 2015; Lencina-Avila et al., 2018; Monteiro, Kerr, & Machado, 2020; Monteiro, Kerr, Orselli, et al., 2020). For this, the following relationship (Equation 1) was applied:

$$\text{TA}(\theta, S); \text{CT}(\theta, S, \text{O}_2), \quad (1)$$

where TA is total alkalinity and CT is total inorganic carbon;  $\theta$  is potential temperature, S is practical salinity, and O<sub>2</sub> is dissolved oxygen. Briefly, measured TA and CT and the respective hydrographic parameters were tested in two groups (i.e., reconstruction and assessment) for some sets to find the best equation suitable for the Bransfield Strait. Overall, we tested three subsets:

1. Set01: a specific set of equations, considering a pair of TA and CT equations for each layer of each basin, resulting in eight pairs of equations for the whole strait. This set did not provide a pair of equations for the deep layer of the western basin because of limited Data Availability.
2. Set02: a general set of equations to increase the input data for reconstruction. A pair of TA and CT equations was tested for each layer of the whole strait, resulting in three pairs of equations for the NAP. The input data were tested through the arrangement of specific years and their different combinations.
3. Set03: a general set of equations as described for Set02 but tested via random combinations.

Different combinations of input data were tested to find the best training data, considering at least 1,000 combinations per set. The equations were evaluated using best correlation, lowest root-mean-square error (RMSE), and higher significance (95% confidence interval;  $p < 0.05$ ) and significant F (high values indicate good representation through a linear regression). Comparisons of different sets for each layer (Figure S3 in Supporting Information S1) and other equations developed for broad ocean areas (Lee et al., 2006; Millero et al., 1998; Takahashi

**Table 1**  
*Reconstruction Equations for Carbonate System Parameters With the Best Fit for This Study*

Layer density ( $\text{kg m}^{-3}$ )	TA ( $\mu\text{mol kg}^{-1}$ )	CT ( $\mu\text{mol kg}^{-1}$ )
Surface $\gamma^n \leq 28.0$	TA = $-31.9*\theta - 54.5*S + 4236$ $r = 0.93$ RMSE = $6.35 \mu\text{mol kg}^{-1}$ $n = 72; p < 0.01$ $F = 247.7$	CT = $-29.3*\theta - 26.1*S - 0.57*O_2 + 3311.5$ $r = 0.95$ RMSE = $8.92 \mu\text{mol kg}^{-1}$ $n = 49; p < 0.01$ $F = 139.2$
Intermediate $28.0 < \gamma^n < 28.27$	TA = $-57.1*\theta + 43.6*S - 2652.3$ $r = 0.93$ RMSE = $6.35 \mu\text{mol kg}^{-1}$ $n = 41; p < 0.01$ $F = 115.0$	CT = $-0.73*\theta + 61.2*S + 1.86*O_2 - 352.1$ $r = 0.91$ RMSE = $8.99 \mu\text{mol kg}^{-1}$ $n = 37; p < 0.01$ $F = 53.8$
Deep $\gamma^n \geq 28.27$	TA = $59.7*\theta - 126.2*S + 6805.3$ $r = 0.86$ RMSE = $6.22 \mu\text{mol kg}^{-1}$ $n = 49; p < 0.01$ $F = 63.1$	CT = $135.9*\theta + 797.8*S + 3.2*O_2 - 26019.9$ $r = 0.91$ RMSE = $9.63 \mu\text{mol kg}^{-1}$ $n = 30; p < 0.01$ $F = 39.86$

*Note.* Statistical data related to each reconstruction are presented along with the respective equation, such as correlation ( $r$ ), root mean square error (RMSE), number of samples used for each reconstruction ( $n$ ),  $p$ -value ( $p$ ), and the significance value ( $F$ , which expresses how many of these data are well represented via linear regressions, with high values meaning best fit via linear regressions). Note that these specific relationships present a RMSE that is about half that of those for broad oceanic areas. Acronyms are: TA—total alkalinity ( $\mu\text{mol kg}^{-1}$ ); CT—total inorganic carbon ( $\mu\text{mol kg}^{-1}$ );  $\theta$ —potential temperature ( $^{\circ}\text{C}$ );  $S$ —salinity (unitless);  $O_2$ —dissolved oxygen ( $\mu\text{mol kg}^{-1}$ ); and  $\gamma^n$ —neutral density ( $\text{kg m}^{-3}$ ).

et al., 2014), including the Arctic Ocean (Arrigo et al., 2010), and regional areas of the Southern Ocean (Hauri et al., 2015; Lencina-Avila et al., 2018; Monteiro, Kerr, & Machado, 2020; Monteiro, Kerr, Orselli, et al., 2020) for TA (Figure S4 in Supporting Information S1) and CT (Figure S5 in Supporting Information S1) were tested. Only equations with the same input data used here were considered in this intercomparison. The best-fitted equations for the Bransfield Strait (Set03) are presented in Table 1. The TA estimates were then validated in surface ( $0.99; p < 0.01; n = 22$ ), intermediate ( $0.99; p < 0.01; n = 19$ ), and deep ( $0.81; p < 0.01; n = 12$ ) layers, as well as CT in surface ( $0.99; p < 0.01, n = 26$ ), intermediate ( $0.96; p < 0.01, n = 17$ ), and deep ( $0.98; p < 0.01, n = 9$ ) layers. This set of equations also presents an uncertainty range related with observation and may be classified as a weather error (i.e., an uncertainty of 10% in the estimation of the dissolved carbonate ion, Newton et al., 2015) and similar residuals (i.e., difference between measured and reconstructed TA and CT) to other studies performing the same methodology (between  $-60$  and  $60 \mu\text{mol kg}^{-1}$ , Figure S6 in Supporting Information S1, Hauck et al., 2010; Lee et al., 2006; Takahashi et al., 2014). Since Set03 represents the natural variability of the carbonate chemistry in the Bransfield Strait, TA and CT were reconstructed over 30 years (1990–2019). Hereafter, only the reconstructed TA and CT are used.

Reconstructed TA and CT data were used as input for CO2Sys v2.1 (Lewis & Wallace, 1998) to estimate the other carbonate system parameters (i.e., pH in seawater scale,  $\text{pH}_{\text{sws}}$ ;  $p\text{CO}_2$  in  $\mu\text{atm}$ ; Revelle Factor;  $\Omega_{\text{ar}}$  and  $\Omega_{\text{ca}}$ ). Here,  $\text{pH}_{\text{sws}}$  was used, which is 0.01 units higher than pH in the total scale ( $\text{pH}_T$ , Millero, 2007). The dissociation constants of carbonic acid by Goyet and Poisson (1989) were used, which are recognized for their good performances in high latitude environments (Kerr, Goyet, et al., 2018; Laika et al., 2009; Lencina-Avila et al., 2018; Wanninkhof et al., 1999). To comprehend the impact of different constant sets on the output data from CO2Sys, a sensitivity test was performed, the results of which are described in the Supplementary Material (Tables S2–S4 in Supporting Information S1). Dickson (1990), Upström (1974), and Perez and Fraga (1987) were used for sulfate, total boron and fluoride constants, respectively. Uncertainties related to this reconstruction were calculated following the error propagation of Orr et al. (2018). For  $p\text{CO}_2$ , it was  $84.8 \pm 5.9$  in the surface layer,  $14.0 \pm 0.7$  in the intermediate layer, and  $102.4 \pm 11.7 \mu\text{atm}$  in the deep layer. Lower uncertainties for  $p\text{CO}_2$  were associated with the intermediate layer (Table S5 in Supporting Information S1). The same pattern described in



$p\text{CO}_2$  is observed for  $[\text{H}^+]$  (a proxy for pH uncertainty),  $\Omega_{\text{ar}}$  and  $\Omega_{\text{ca}}$ , for which uncertainties are at an order of magnitude lower in intermediate layers than in surface and deep layers (Table S5 in Supporting Information S1).

### 3.4. Temporal and Climate Composition Approach of Carbonate System Parameters

Interannual variability was assessed by long-term trends ( $\pm$ confidence bounds) based on time series anomalies for each density layer and basin of the Bransfield Strait, following Dotto et al. (2016). Annual anomalies were calculated as annual averages minus the 2010s average because this decade has the higher temporal coverage. Annual trends were statistically significant when the confidence bound was less than the trend value (i.e., 95% confidence level;  $p < 0.05$ ).

Decadal variability was assessed through decadal averaged ( $\pm$ standard error) vertical profiles for the carbonate system parameters at bins of 50 m over the three decades (i.e., the 1990s during 1990–1999, 2000s during 2000–2009, and 2010s during 2010–2019, Table S6 in Supporting Information S1). Each calculated average depth level in the vertical profile was assessed, point by point, through the Mann-Whitney test to identify significant differences among these three decades, considering a significance level of 95% ( $p < 0.05$ ).

Vertical variability was also assessed through a composite analysis, which evaluated the role played by ENSO ([https://origin.cpc.ncep.noaa.gov/products/analysis\\_monitoring/ensostuff/ONI\\_v5.php](https://origin.cpc.ncep.noaa.gov/products/analysis_monitoring/ensostuff/ONI_v5.php), last access: 13 November 2022) and SAM (<http://www.nerc-bas.ac.uk/icd/gjma/sam.html>, last access: 13 November 2022) and their effects on carbonate chemistry within the strait. Their effects were evaluated over summers (January, February, and March) in its negative (index  $\leq -0.5$ , SAM–/ENSO–), neutral ( $-0.5 < \text{index} < 0.5$ , SAMn/ENSON), and positive (index  $\geq 0.5$ , SAM+/ENSO+) phases. Differences for composite analysis were tested for significance by the Mann-Whitney test for each depth interval of 50 m in each basin. Each vertical profile shown here represents a composite profile.

## 4. Results

### 4.1. Western Basin of the Bransfield Strait

The surface layer of the western basin was characterized by annual average  $\pm$  standard error varying from  $2,315 \pm 2$  to  $2,381 \pm 1 \mu\text{mol kg}^{-1}$  for TA and  $2,195 \pm 1$  to  $2,291 \pm 1 \mu\text{mol kg}^{-1}$  for CT (Figures S7a and S7b in Supporting Information S1). The surface averages of  $\text{pH}_{\text{sws}}$ ,  $\Omega_{\text{ar}}$ , and  $\Omega_{\text{ca}}$ , reaching  $8.141 \pm 0.001$ ,  $1.78 \pm 0.01$ , and  $2.80 \pm 0.01$ , respectively (Figures S7d–S7f in Supporting Information S1), were higher than those in the intermediate and deep layers. The total average (i.e., average over the whole data set) of  $p\text{CO}_2$  was higher in the intermediate layer with  $542.7 \pm 2.0 \mu\text{atm}$ , likely associated with modified-CDW intrusions. Furthermore, total averages of  $\text{pH}_{\text{sws}}$ ,  $\Omega_{\text{ar}}$ , and  $\Omega_{\text{ca}}$  in the intermediate layer were  $7.917 \pm 0.002$  (minimum of 7.8),  $1.03 \pm 0.01$  (minimum of 0.7), and  $1.61 \pm 0.01$  (minimum of 1.1), respectively (Figure S7 in Supporting Information S1). The TA annual-average vertical distribution was lower in the intermediate layer ( $2,276 \pm 1 \mu\text{mol kg}^{-1}$ ) relative to the surface layer and reached  $2,392 \pm 0.1 \mu\text{mol kg}^{-1}$  in the deep layer (Figure S7 in Supporting Information S1). Annual averaged CT increased with depth, reaching  $2,300 \pm 1 \mu\text{mol kg}^{-1}$  in the deep layer (Figure S7 in Supporting Information S1).

In general, interannual variability showed steeper and more significant trends in the deepest layers, except for TA (Table 2, Figure S8a in Supporting Information S1). The deep layer had a sharp positive trend for CT per year, threefold higher than that in the intermediate layer (Table 2, Figure S8b in Supporting Information S1). Although data were solely restricted to the 2010s for the deep layer of the western basin, the CT trend was well-marked due to the high variability. Moreover, the annual trend for  $p\text{CO}_2$  in the deep layer also showed a sharp positive trend of  $18 \pm 9 \mu\text{atm yr}^{-1}$ , being ninefold higher than that at the surface (Table 2). Interannual trends showed a clear reduction per year for  $\text{pH}_{\text{sws}}$ ,  $\Omega_{\text{ar}}$ , and  $\Omega_{\text{ca}}$ , which increase with depth and characterize the deep layer with trends up to three- and fivefold higher than for the intermediate and surface layers, respectively (Table 2).

Decadal-average vertical profiles of TA and CT showed no long-term variability in the surface layer (Figures 2a and 2b,  $p > 0.05$ , Table S8 in Supporting Information S1). However, TA and CT decreased between the 1990s and 2000s ( $p < 0.01$ , Table S8 in Supporting Information S1) for the intermediate layer around 450–1,000 m (Figures 2a and 2b). During the 2010s, TA and CT recovered to values of the 1990s ( $p < 0.01$ , Table S8 in Supporting Information S1). A progressive increase in  $p\text{CO}_2$  values below 200 m was observed from the 1990s to

**Table 2**
*Trends ± Confidence Bound for Carbonate System Parameters Based on a Time Series of 30 Years of Reconstructed Data During 1990–2019 in the Bransfield Strait*

Layer	Basin	Period of TA data (other parameters)	TA ( $\mu\text{mol kg}^{-1} \text{ yr}^{-1}$ )	CT ( $\mu\text{mol kg}^{-1} \text{ yr}^{-1}$ )	$p\text{CO}_2$ ( $\mu\text{atm yr}^{-1}$ )	$\text{pH}_{\text{sws}}$ ( $\text{pH}_{\text{sws}}$ units $\text{yr}^{-1}$ )	$\Omega_{\text{ar}}$ ( $\text{yr}^{-1}$ )	$\Omega_{\text{ca}}$ ( $\text{yr}^{-1}$ )
Surface	Western	1990–2019 (1996–2019)	$-0.10 \pm 0.23$	$0.09 \pm 0.51$	$2.11 \pm 2.70$	<b><math>-0.003 \pm 0.002</math></b>	<b><math>-0.010 \pm 0.006</math></b>	<b><math>-0.015 \pm 0.010</math></b>
	Central	1990–2019 (2000–2019)	$-0.17 \pm 0.27$	<b><math>-0.92 \pm 0.82</math></b>	$-0.33 \pm 0.66$	$0.0004 \pm 0.0007$	$0.001 \pm 0.002$	$0.002 \pm 0.004$
	Eastern	1999–2019 (1999–2019)	<b><math>-0.25 \pm 0.11</math></b>	<b><math>-0.34 \pm 0.26</math></b>	<b><math>0.23 \pm 0.09</math></b>	<b><math>-0.0002 \pm 0.0001</math></b>	$-0.0003 \pm 0.0004$	$-0.0004 \pm 0.0006$
Intermediate	Western	1990–2019 (1996–2019)	<b><math>0.46 \pm 0.40</math></b>	$2.47 \pm 3.27$	<b><math>8.34 \pm 7.86</math></b>	<b><math>-0.008 \pm 0.002</math></b>	<b><math>-0.018 \pm 0.009</math></b>	<b><math>-0.029 \pm 0.014</math></b>
	Central	1990–2019 (2000–2019)	<b><math>0.49 \pm 0.20</math></b>	$1.00 \pm 1.05$	$0.95 \pm 4.88$	$0.0004 \pm 0.0036$	$0.004 \pm 0.007$	$0.005 \pm 0.011$
	Eastern	1999–2019 (1999–2019)	$-0.37 \pm 0.43$	$-0.30 \pm 0.37$	<b><math>0.36 \pm 0.36</math></b>	<b><math>0.0002 \pm 0.0001</math></b>	<b><math>0.0006 \pm 0.0003</math></b>	<b><math>0.0009 \pm 0.0006</math></b>
Deep	Western	1990–2019 (2013–2019)	$0.10 \pm 0.24$	<b><math>6.77 \pm 3.76</math></b>	<b><math>17.98 \pm 8.99</math></b>	<b><math>-0.017 \pm 0.010</math></b>	<b><math>-0.044 \pm 0.027</math></b>	<b><math>-0.070 \pm 0.043</math></b>
	Central	1990–2019 (2000–2019)	<b><math>-0.42 \pm 0.15</math></b>	$-0.18 \pm 2.29$	$-0.81 \pm 6.90$	$0.0007 \pm 0.0062$	$0.002 \pm 0.011$	$0.003 \pm 0.018$
	Eastern	1999–2019 (1999–2019)	$-0.14 \pm 0.21$	<b><math>-0.48 \pm 0.47</math></b>	<b><math>-0.31 \pm 0.15</math></b>	<b><math>0.0003 \pm 0.0001</math></b>	<b><math>0.0007 \pm 0.0002</math></b>	<b><math>0.0010 \pm 0.0004</math></b>

Note. If the confidence bound is higher than the trend, the trend is not statistically significant (i.e.,  $p > 0.05$ ; 95% confidence interval). Significant values are highlighted in bold.

the 2010s, consequently related to concurrent  $\text{pH}_{\text{sws}}$  and  $\Omega_{\text{ar}}$  and  $\Omega_{\text{ca}}$  reductions (Figures 2c–2f). It is noted that the vertical distribution of carbonate system parameters was mainly affected by both ENSO and SAM (Figure 3 and Figure S8 in Supporting Information S1). During SAM– (Figure 3b) and ENSO+ (Figure 3d), CT below ~350 m increased when compared to the vertical distribution observed in years marked by a neutral phase. Furthermore, although changes were noted in TA and CT concentrations,  $p\text{CO}_2$ ,  $\text{pH}_{\text{sws}}$ ,  $\Omega_{\text{ar}}$ , and  $\Omega_{\text{ca}}$  experienced well-marked changes between 300 and 500 m in depth during SAM– and ENSO+, in which TA and CT changes were associated with  $p\text{CO}_2$  increase, and  $\text{pH}_{\text{sws}}$ ,  $\Omega_{\text{ar}}$  and  $\Omega_{\text{ca}}$  decrease (Figure S9 in Supporting Information S1).

## 4.2. Central Basin of the Bransfield Strait

The surface layer of the central basin had total average concentrations for TA and CT of  $2368 \pm 1$  and  $2243 \pm 2 \mu\text{mol kg}^{-1}$ , respectively (Figures S10a and S10b in Supporting Information S1), which are close to those of the surface waters of the western basin (Figures S7a and S7b in Supporting Information S1). The total average value of  $p\text{CO}_2$  in the surface layer was  $394.8 \pm 4.0 \mu\text{atm}$ , whereas  $\text{pH}_{\text{sws}}$ ,  $\Omega_{\text{ar}}$ , and  $\Omega_{\text{ca}}$  were  $8.121 \pm 0.001$ ,  $1.70 \pm 0.01$ , and  $2.71 \pm 0.01$ , respectively (Figure S11 in Supporting Information S1). The average values in the intermediate layer were marked by a minimum annual average for  $\text{pH}_{\text{sws}}$  of  $7.758 \pm 0.002$  and a maximum for  $p\text{CO}_2$  of  $750.2 \pm 3.5 \mu\text{atm}$  relative to the other layers in the basin (Figure S10 in Supporting Information S1). Low TA and CT variabilities were observed for the whole water column, with the total average varying from 10 in the surface to  $13 \mu\text{mol kg}^{-1}$  deep layer. The average values of  $\Omega_{\text{ar}}$  and  $\Omega_{\text{ca}}$  decreased with depth, with  $\Omega_{\text{ar}}$  reaching subsaturated condition in most of the vertical profiles and  $\Omega_{\text{ca}}$  in a few in the deep layer (Figure S10 in Supporting Information S1).

Increasing TA and CT trends were observed only in the intermediate layer (Table 2, Figure S11 in Supporting Information S1), with CT, in particular, showing higher interannual variability (Figure S11b in Supporting Information S1). Although with no significant trends,  $\text{pH}_{\text{sws}}$ ,  $\Omega_{\text{ar}}$ , and  $\Omega_{\text{ca}}$  increased in the entire water column for the studied period (Table 2, Figure S11 in Supporting Information S1). Unfortunately, the carbonate chemistry reconstruction is limited to those years with available hydrographic data, restricting a better spatiotemporal coverage in the 1990s in this basin.

The last 30 years have been marked by a  $p\text{CO}_2$  increase and simultaneous  $\text{pH}_{\text{sws}}$ ,  $\Omega_{\text{ar}}$ , and  $\Omega_{\text{ca}}$  decrease over the last two decades in the entire vertical profile (Figures 4c–4f). Particularly for  $\Omega_{\text{ar}}$ , depths below 200 m were below

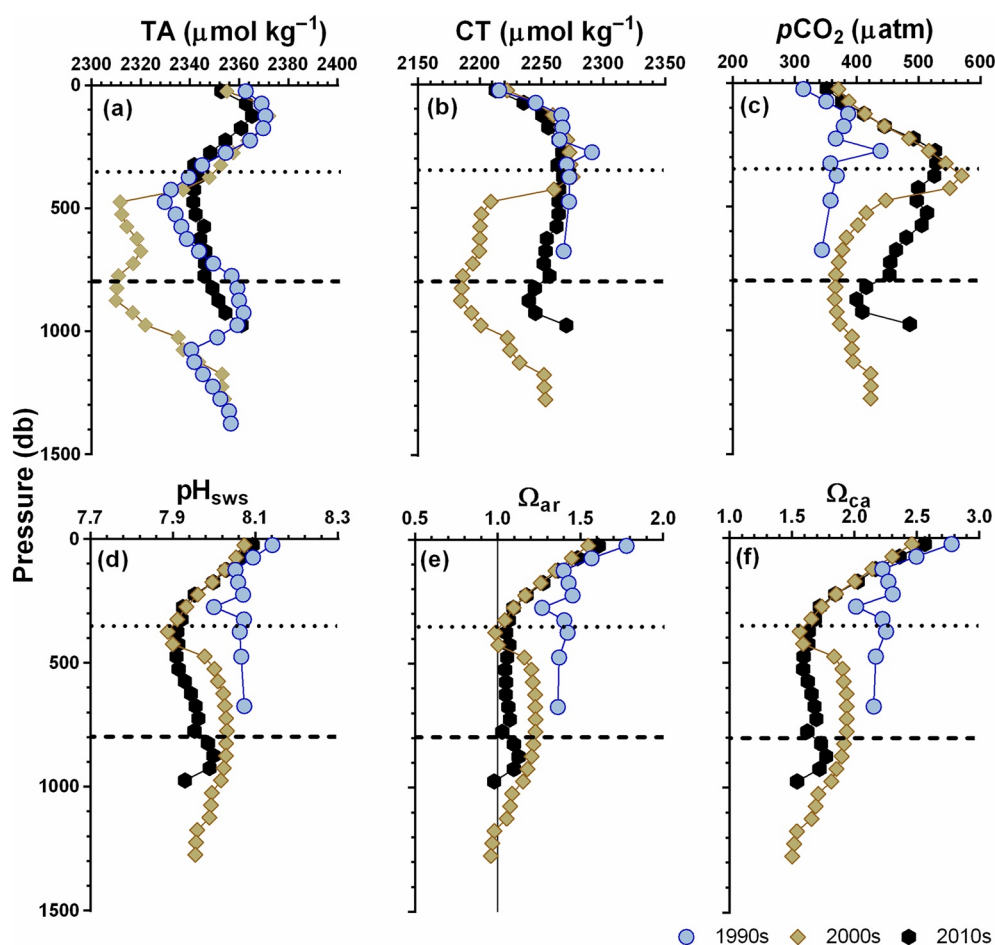


**Figure 2.** Vertical profiles of decadal averages of carbonate system parameters in the western basin of the Bransfield Strait during 1990–2019 for total alkalinity (TA) and during 1996–2019 for the other parameters. Plotted data are (a) total alkalinity—TA, (b) total inorganic carbon—CT, (c) partial pressure of carbon dioxide— $p\text{CO}_2$ , (d)  $\text{pH}_{\text{sws}}$  (seawater scale), (e) aragonite saturation state— $\Omega_{\text{ar}}$ , and (f) calcite saturation state— $\Omega_{\text{ca}}$ . The averaged values are calculated for 50-m bins until the deepest sample in each decade. The total standard errors for the data were  $<1.9$  for TA,  $<2.4 \mu\text{mol kg}^{-1}$  for CT,  $<5.2 \mu\text{atm}$  for  $p\text{CO}_2$ ,  $<0.004 \text{ pH}_{\text{sws}}$  units, and  $<0.04$  for both  $\Omega_{\text{ar}}$  and  $\Omega_{\text{ca}}$ . The black horizontal dotted and dashed lines in the panels represent the average value of the neutral density ( $\gamma_n$ ) levels of 28.00 and 28.27  $\text{kg m}^{-3}$ , respectively. The vertical line in panel (e) indicates  $\Omega_{\text{ar}} = 1$ , with values below 1 referring to subsaturation of calcium carbonate. Only the 2010s presented  $\gamma_n$ , with the value 28.27  $\text{kg m}^{-3}$ , to characterize the deep layer in this basin for CT and the other  $\text{CO}_2$ -carbonate system parameters, except for TA.

saturation conditions (i.e.,  $\Omega_{\text{ar}} < 1$ ) in the 2010s (Figure 4e). Furthermore, TA was constant over decades and during any SAM and ENSO events (Figures 3e and 3g, respectively). The  $\text{pH}_{\text{sws}}$ ,  $\Omega_{\text{ar}}$  and  $\Omega_{\text{ca}}$  were lowest in the deep layer during SAM+ and SAM− events compared to SAMn and ENSO+ (Figures S9b–S9h in Supporting Information S1).

### 4.3. Eastern Basin of the Bransfield Strait

The eastern basin is filled with water masses with relative homogeneity in the vertical distribution of carbonate chemistry, which implies low interannual and decadal variability (Figures S12–S14 in Supporting Information S1). Interannual trends were small in the eastern basin compared to the other basins of the strait, and most carbonate system parameters had a negative trend although low temporal variability (Table 2, Figure S12 in Supporting Information S1). However, at surface levels,  $p\text{CO}_2$  increased over time at a trend of  $0.23 \pm 0.10 \mu\text{atm yr}^{-1}$ , while  $\text{pH}_{\text{sws}}$ ,  $\Omega_{\text{ar}}$ , and  $\Omega_{\text{ca}}$  in the deepest layers also exhibited positive trends of  $0.0003 \pm 0.0001 \text{ pH}_{\text{sws}}$  units  $\text{yr}^{-1}$ ,  $0.0007 \pm 0.0002 \Omega_{\text{ar}}$  units  $\text{yr}^{-1}$  and  $0.0010 \pm 0.0004 \Omega_{\text{ca}}$  units  $\text{yr}^{-1}$ , respectively (Table 2, Figure S12 in Supporting Information S1).

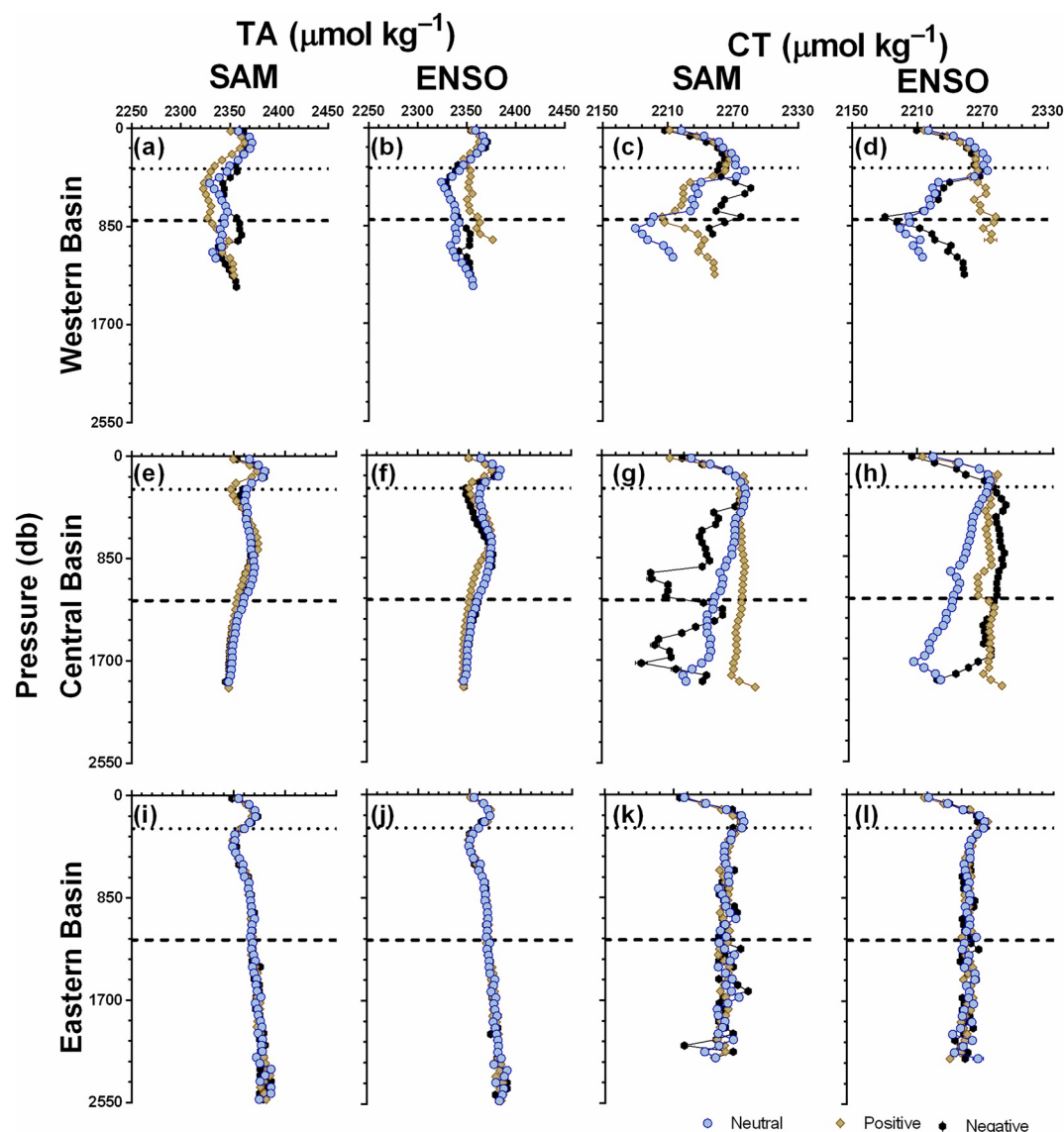


**Figure 3.** Compositing vertical profiles of (a, b, e, f, i, and j) total alkalinity—TA ( $\mu\text{mol kg}^{-1}$ ) and (c, d, g, h, k, and l) total inorganic carbon—CT ( $\mu\text{mol kg}^{-1}$ ) considering the phases of the modes of climate variability Southern Annular Mode (SAM, first and third columns) and El Niño-Southern Oscillation (ENSO, second and fourth columns). Averaged TA and CT profiles for the (first arrow: a–d) western, (second arrow: e–h) central, and (third arrow: i–l) eastern basins of Bransfield Strait. SAMn includes 1996, 2004, 2011, and 2014 in the western basin; 1996, 1999, 2004, 2011, and 2014 in the central basin; and 1999, 2003, 2004, 2006, 2008, 2011, and 2014 in the eastern basin. SAM+ includes 1990, 1997, 2013, 2015, 2016, 2018, and 2019 in the western basin; 1990, 1997, 1998, 2000, 2005, 2008, 2009, 2013, 2015, 2016, 2018, and 2019 in the central basin; and 2005, 2009, 2013, 2015, 2016, 2018, and 2019 in the eastern basin. SAM– includes 1993, 2010, and 2017 in the western basin; 2003, 2010, and 2017 in the central basin; and 2010 and 2017 in the eastern basin. ENSOn includes 1990, 1993, 1997, 2004, 2014, and 2017 in the western basin; 1990, 1997, 2000, 2004, 2013, 2014, and 2017 in the central basin; and 2004, 2006, 2013, 2014, and 2017 in the eastern basin. ENSO+ includes 2010, 2015, 2016, and 2019 in the western basin; 2003, 2010, 2015, 2016, and 2019 in the central basin; and 2003, 2005, 2010, 2015, 2016, and 2019 in the eastern basin. ENSO– includes 1996, 2008, 2011, 2013, and 2018 in the western basin; 1996, 1998, 1999, 2008, 2009, 2011, and 2018 in the central basin; and 1999, 2008, 2009, 2011, and 2018 in the eastern basin.

## 5. Discussion

### 5.1. What Drives Carbonate System Variability in the Bransfield Strait?

The temporal and spatial variability of carbonate chemistry in the Bransfield Strait evolves based on changes related to water mass intrusions in the region. Hydrographic and chemical changes in the water column structure

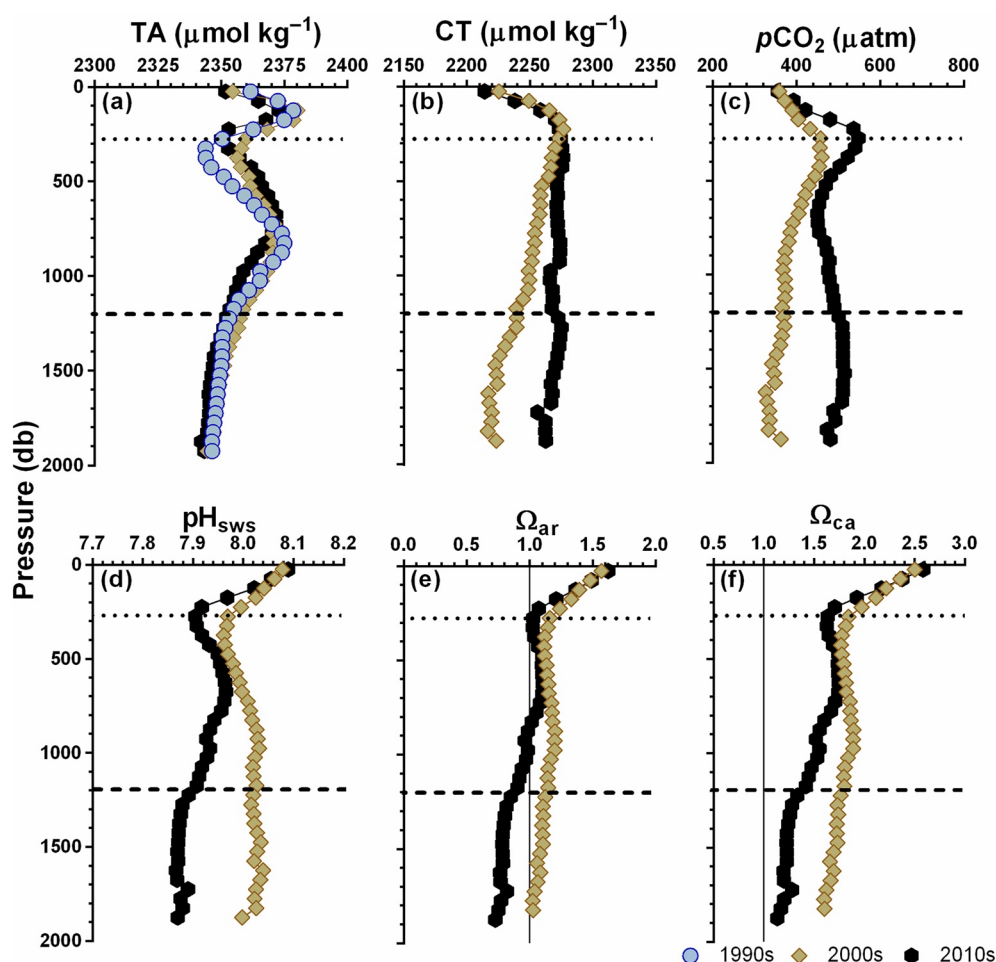


**Figure 4.** Vertical profiles of decadal averages for carbonate system parameters in the central basin of Bransfield Strait during 1990–2019 for total alkalinity (TA) and during 2000–2019 for the other parameters. Data plotted are (a) total alkalinity—TA, (b) total inorganic carbon—CT, (c) partial pressure of carbon dioxide— $p\text{CO}_2$ , (d)  $\text{pH}_{\text{sws}}$  (seawater scale), (e) aragonite saturation state— $\Omega_{\text{ar}}$ , and (f) calcite saturation state— $\Omega_{\text{ca}}$ . The averaged values are calculated for 50-m bins until the deepest sample in each decade. The total standard errors for the data were  $<1.2$  for TA,  $<1.5 \mu\text{mol kg}^{-1}$  for CT,  $<5.3 \mu\text{atm}$  for  $p\text{CO}_2$ ,  $<0.005$  for  $\text{pH}_{\text{sws}}$ , and  $<0.02$  for both  $\Omega_{\text{ar}}$  and  $\Omega_{\text{ca}}$ . The solid vertical line in panels (e) and (f) indicates  $\Omega_{\text{ar}} = 1$  and  $\Omega_{\text{ca}} = 1$ , respectively, with values below 1 referring to subsaturation of calcium carbonate.

respond to the interactions of ENSO and SAM (Avelina et al., 2020; Loeb et al., 2009; Renner et al., 2012; Ruiz Barlett et al., 2018; van Caspel et al., 2018), which regulate the main source water mass that intrudes into the region (Damini et al., 2022; Wang et al., 2022). This occurs due to the variability of modified-CDW from the western Antarctic Peninsula (i.e., a relatively old, warm, salty, less oxygenated, and TA- and CT- rich water mass) and DSW from the eastern Antarctic Peninsula (i.e., a recently ventilated, cold, salty, high oxygenated, and TA- and CT- rich water mass). However, the magnitude of the mixing processes along the water column depends on the ocean dynamics and bathymetry of each basin of the Bransfield Strait. While the western and eastern basins of the strait are more exposed to receiving a higher amount of modified-CDW intrusions at intermediate levels, the same is not true for the central basin because the Bransfield Gyre tends to constrain this water mass toward the South Shetland Islands (Huneke et al., 2016; Sangrà et al., 2011). In addition, the purest form of DSW (i.e., less mixing with ambient waters) is mainly constrained in the central basin at deep levels after sinking into the region (Damini et al., 2022; Dotto et al., 2016).

Interannual and decadal variabilities in the western basin of the Bransfield Strait (Figure S12 in Supporting Information S1) respond to the dynamics of the Antarctic Circumpolar Current and the modes of climate variability prevailing over time. For example, during the early 2000s, both SAM+ and ENSOn/ENSO- were characterized by increasing modified-CDW intrusions (Loeb et al., 2009; Renner et al., 2012), mainly up to 500 m in depth,



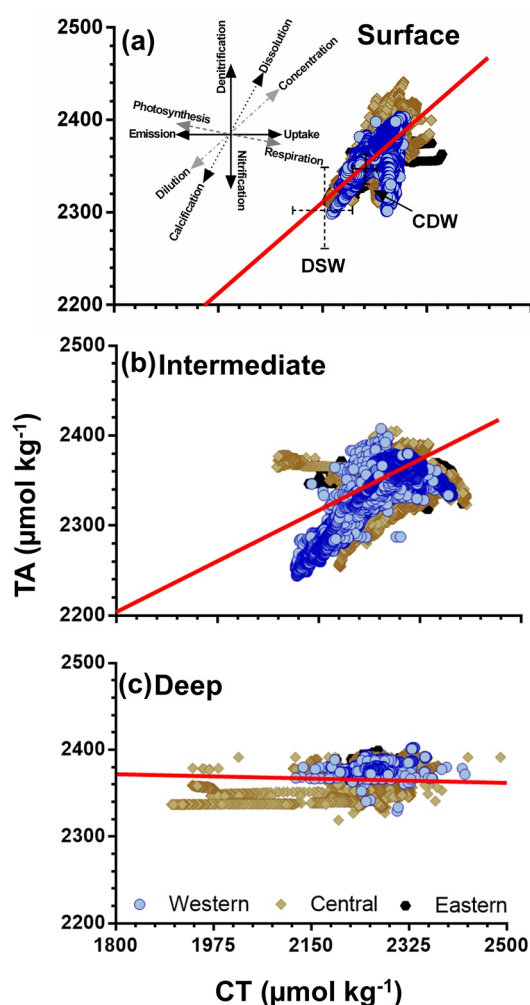


**Figure 5.** Dispersal diagram of the relationship between total inorganic carbon (CT) and total alkalinity (TA) for the (a) surface, (b) intermediate, and (c) deep layers of the Bransfield Strait. The arrows in the inset (a) represent the TA:CT ratio, which characterizes the physical-biogeochemical processes that affect parameters (based on Zeebe and Wolf-Gladrow (2001)). Such processes are as follows: denitrification/nitrification (changes only in TA), concentration/dilution due to freshwater removal/input (changing TA and CT in a 1:1 ratio), and photosynthesis/decomposition (changing TA and CT in a 0.14:1 ratio). The colors and symbols differ among basins, as indicated in panel (c). The red lines show the linear regression between CT and TA in the surface ( $n = 95108$ ;  $TA = 0.555 (\pm 0.002) * CT + 1,119$ ;  $p < 0.001$ ), intermediate ( $n = 150706$ ;  $TA = 0.323 (\pm 0.001) * CT + 1,624$ ;  $p < 0.001$ ), and deep ( $n = 99684$ ;  $TA = -0.017 (\pm 0.001) * CT + 2,403$ ;  $p < 0.001$ ) layers. The end-members of the TA and CT source water masses were marked by the crosses in panel (a) and were selected from Broullón et al. (2019, 2020), respectively. The source water masses are Circumpolar Deep Water in the open ocean near the western Antarctic Peninsula and Dense Shelf Water in the north-western Weddell Sea.

in the western Antarctic Peninsula continental shelf (Moffat et al., 2009; Wang et al., 2022). Because the origin of modified-CDW implies high TA and CT concentrations, it should be associated with a concurrent rise in TA and CT, but this is not the case. The heat transported alongside by the intense modified-CDW intrusions during periods of SAM+, which reach the coastal areas of Antarctica, influences glacial retraction with consequent meltwater input into the ocean (Abernathy et al., 2016; Meredith et al., 2008, 2014; Shepherd et al., 2004, 2018). The freshwater input and the consequent dilution may contribute with a characteristic signature (i.e., low TA and CT relative to surrounding seawater) to the surface layer of the western basin of the Bransfield Strait, which eventually is advected from the western Antarctic Peninsula (Moffat & Meredith, 2018; Shepherd et al., 2018) into the water column because of the vertical mixing (Gille, 2008). This dilution is a possible countereffect of the high TA and CT content associated with the modified-CDW, but with no or minimized impact on  $pCO_2$ ,  $pH_{sws}$ ,  $\Omega_{ar}$ , and  $\Omega_{ca}$  (Figure 2). Indeed, the meltwater contribution may reduce TA and CT up to 1,000 m in depth (Figures 2a and 2b) as previously detected on the western Antarctic Peninsula (Legge et al., 2017; Lencina-Avila et al., 2018). As long as SAM+ events have been more frequent over recent decades (Marshall et al., 2006), negative trends for TA and CT due to dilution, but intensification of  $pCO_2$ ,  $pH_{sws}$ ,  $\Omega_{ar}$ , and  $\Omega_{ca}$  trends (Table 2) may become marked over time if melting contributions become more intense.

The central and eastern basins showed a less intense influence of modified-CDW intrusions, which may be significant to achieve a TA:CT ratio similar to the ones for the upper layers from the western basin. The dispersion of TA and CT and the ratio between these parameters can be used to diagnose the processes influencing them (Figure 5a) because each process alters TA and CT with a certain ratio (Zeebe & Wolf-Gladrow, 2001). In this case, modified-CDW intrusions might capture the meltwater signature from Antarctic Surface Water in the western Antarctic Peninsula through its mixture with CDW and promote a dilution/concentration signature for TA:CT ratios (see the inset in Figure 5a for theoretical ratios). Thus, the presence and variability of modified-CDW intrusions into the surface and intermediate layers in the Bransfield Strait contribute to the key process driving carbonate chemistry variability through dilution and concentration of salts (Figures 5a and 5b).

However, DSW is the main water mass filling the water column below 500 m in the Bransfield Strait (Damini et al., 2022), which controls the rapid changes of carbonate system parameters in deep layers. In the western basin, the deep layer showed a positive trend for DSW contribution over the last decade (Ruiz Barlett et al., 2018). Its high carbon signature, added to the mixing with modified-CDW, may be associated with the sharp positive trend of CT (Table 2). Positive trends of carbonate system parameters associated with modified-CDW intrusions were also observed in the southern Gerlache Strait and DSW in the northern Gerlache Strait (Lencina-Avila et al., 2018), as well as in the deep layers of the Weddell Sea (van Heuven et al., 2014).

For the central and eastern basins, DSW contributed up to ~60% to the mixture of source water masses filling the deep layers (Damini et al., 2022).

This water sinks from the shallow shelf zones directly to the seafloor as dense and cold plumes flow down the sills, a ventilation process with relatively low mixing with surrounding waters (Dotto et al., 2016; van Caspel et al., 2018). Thus, this process advects DSW properties from the north-western Weddell Sea continental shelf

into the Bransfield Strait. In fact, the Bransfield Front also acts to constrain the contributions of modified-CDW close to the South Shetland Islands.

The presence of DSW may intensify interannual trends or decadal variability of CT and  $p\text{CO}_2$  and decrease  $\text{pH}_{\text{sws}}$ ,  $\Omega_{\text{ar}}$ , and  $\Omega_{\text{ca}}$  in the deep layer in both western (Table 2) and central (Figure 4) basins, respectively. Beyond natural  $\text{CO}_2$ , the DSW may transport anthropogenic carbon westward, such as previously observed by Kerr, Goyet et al. (2018) in the Gerlache Strait. In addition, unpublished data by GOAL has shown that the estimated anthropogenic carbon concentration reached up to  $50 \mu\text{mol kg}^{-1}$  in the central basin of the Bransfield Strait in the late 2010s, which are contributions expected for shelf waters around Antarctica (Pardo et al., 2014). Curiously, CT anomalies (Figure S12 in Supporting Information S1) vary fourfold more than anthropogenic carbon estimates around the NAP ( $\sim 20 \mu\text{mol kg}^{-1}$ , Kerr, Goyet, et al., 2018; Lencina-Avila et al., 2018), which may indicate a contribution of this carbon fraction on carbonate chemistry. Regardless of whether natural  $\text{CO}_2$  or anthropogenic carbon dissolves into the surface of the north-western Weddell Sea, the rapid ventilation of DSW does not allow the equilibrium of  $\text{CO}_2$  concentration between the ocean and the atmosphere to be reached. This implies that DSW ventilation advects a fraction of the whole  $\text{CO}_2$  available to be captured before inflowing into the Bransfield Strait, promoting high CT and  $p\text{CO}_2$  variability over time, as observed in Figures S11b and S11c in Supporting Information S1, respectively. Thus, the advection of DSW throughout the Bransfield Strait can act as an uptake signature (i.e., altering CT with no TA change; see the inset in Figure 5a for theoretical ratios). However, the magnitude of anthropogenic carbon inputs and their role over the long-term in the Bransfield Strait have not yet been assessed.

The complexity of the deep basins is intensified by organic matter cycling in the Bransfield Strait. High primary productivity takes place in the north-western Weddell Sea (Detoni et al., 2015; Ito et al., 2018; Mendes et al., 2012), transporting organic matter in DSW into the deepest layers of the Bransfield Strait, where it may be decomposed. This transport was previously indicated by Avelina et al. (2020) when evaluating dissolved organic carbon in the central basin of the Bransfield Strait in 2015. Organic matter decomposition is associated with increases in CT and  $p\text{CO}_2$  and reductions in TA,  $\text{pH}_{\text{sws}}$ ,  $\Omega_{\text{ar}}$ , and  $\Omega_{\text{ca}}$ , as noticed in the central basin in the 2010s relative to the 2000s (Figure 4). Although multivariate linear equations may capture a low signal of TA changes related to organic matter decomposition (Lee et al., 2006), all the features mentioned above may corroborate this driver of carbonate chemistry variability in the deep layer of the central basin.

## 5.2. Inferred Processes Controlling Carbonate Chemistry in the Bransfield Strait: A Possible Broad Avenue for Future Studies

As multivariate linear equations capture changes in  $\theta$ , S, and  $\text{O}_2$  associated with processes controlling TA and CT changes, such as freshwater input and biological processes, the results presented here point out other possible processes controlling carbonate chemistry in the Bransfield Strait. This new avenue for further investigation is highlighted by the evidence found here and described below.

First, it is well known that changes in the cryosphere system (e.g., sea ice variability and continental meltwater input) and other hydrographic dynamics can affect the carbonate system variability through changes in salinity (e.g., Henley et al., 2019; Orselli et al., 2022). Freshwater input or removal can alter TA and CT. Indeed, the Antarctic Peninsula has recently been losing several ice shelves through extreme events of heat waves, atmospheric rivers and the abrupt collapse of Larsen A and B (Massom et al., 2018; Reid & Massom, 2022; Scambos et al., 2000; Wille et al., 2022). Besides, Dotto et al. (2016) identified a change of nearly 0.06 units of salinity over the last 60 years, while our study points out a reduction of 0.02 units of salinity between the 2000s and 2010s in the deep layer of the central basin. Even if this change is considered small, it may impact TA in the long term. Thus, the carbonate chemistry in the Bransfield Strait is directly affected by this freshwater input.

Additionally, Gordon et al. (2000) and von Gyldenfeldt et al. (2002) indicate that the water mass contribution from the Ronne-Filchner ice shelf (southern Weddell Sea) overflows by a sill in the vicinity of the Powell Basin into the deep layer of the eastern basin of the Bransfield Strait. Due to its low temperature (Frölicher et al., 2015; Hellmer et al., 2017) and low anthropogenic carbon content (Pardo et al., 2014), this water mass has the potential to minimize the effects of anthropogenic carbon carried by DSW into the deep layer, promoting increases of  $\text{pH}_{\text{sws}}$  values as a thermal effect. However, the eastern basin has been a challenging area for both hydrographic and biogeochemical assessments.

Second, local processes may also contribute to the variability of the carbonate system in the Bransfield Strait. For example, the presence of hydrothermal vents and volcanos at the bottom of the strait (Almendros et al., 2020) could be correlated with chemosynthesis processes, which can alter TA and CT by a ratio between  $\text{CO}_2$  ingassing and organic matter decomposition (Figure 5c). In addition, the release of  $\text{CO}_2$  through hydrothermal vents may act as a direct process of  $\text{CO}_2$  ingassing process into the water column with no TA change (Figure 5c). The latter can help to explain the distribution of the TA:CT distribution observed in the deep layers of the Bransfield Strait since this pattern is expected in surface waters (Figure 5c and inset in Figure 5a). Furthermore, the increase in CT may be enhanced by anthropogenic carbon intrusion through advected DSW (Kerr, Goyet, et al., 2018), although anthropogenic carbon storage in the Bransfield Strait remains unclear. Indeed, several biological, chemical and geological processes are occurring concomitantly in the deep layers, holding a TA:CT ratio between organic matter decomposition and close to that expected at the ocean-atmosphere interface (Figure 5c). These processes acting as  $\text{CO}_2$  inputs into the deep layer in the entire strait might enhance uncertainties for  $p\text{CO}_2$ , as observed in the present study (Table S5 in Supporting Information S1).

Finally, evidence of nitrification in the deep layer might be another biogeochemical process with impacts on carbonate chemistry (Figure S15 in Supporting Information S1). This is characterized by changes in TA as observed in the central basin and as described by Wolf-Gladrow et al. (2007). Nitrifying organisms, such as archaea of the genus *Thaumarchaeota*, occur in the Southern Ocean, including the Bransfield Strait (Signori et al., 2014). Since this evidence is identified in SAM+, warm sea surface temperature in the Weddell Sea may favor high levels of nutrients, such as ammonium and nitrite, being advected into the deep layer of the central basin. Moreover, high  $\text{O}_2$  concentrations in DSW (Avelina et al., 2020) are another needful feature for nitrification. According to all of the theoretical evidence above, if nitrification processes take place in the Bransfield Strait, they could potentially influence the carbonate chemistry. However, further investigations are required to understand the magnitude of nitrification around the NAP and its impact on carbonate chemistry.

### 5.3. Acidification Process and Carbon Dioxide Saturation in the Bransfield Strait

Spatial and temporal variability of carbonate system parameters in the Bransfield Strait weighs changes in  $\text{pH}_{\text{sws}}$ ,  $\Omega_{\text{ar}}$  and  $\Omega_{\text{ca}}$ , which vary in trend and magnitude among basins (Table 2, Figures S9, S12, and S13 in Supporting Information S1). The western basin may be associated with the strongest negative trends (Table 2, Figure S9d in Supporting Information S1) because of an increasing frequency of CDW intrusions, highlighting a contribution of a natural process to pH trends. For instance, the surface layer of the western basin has trends ( $-0.003 \pm 0.002 \text{ pH}_{\text{sws}} \text{ units yr}^{-1}$ , Table 2) similar to those of the deep layer of the northern Gerlache Strait ( $-0.003 \pm 0.001 \text{ pH}_{\text{sws}} \text{ units yr}^{-1}$ , Lencina-Avila et al., 2018), central western Antarctic Peninsula ( $0.002 \pm 0.002 \text{ pH}_T \text{ units yr}^{-1}$ , Hauri et al., 2015), and the surface layer of the Southern Ocean ( $-0.002 \pm 0.0003 \text{ pH}_T \text{ units yr}^{-1}$ , Midorikawa et al., 2012). However, these trends observed surrounding the Antarctic Peninsula are smaller than those found in other sensitive regions, exhibiting a high Revelle Factor (Jiang et al., 2019; Sabine et al., 2004), such as the North Sea (Blackford & Gilbert, 2007). Adding up the trends of other areas of the Southern Ocean, such as the one for the south area of the Polar Front ( $-0.0022 \pm 0.0004 \text{ pH}_T \text{ units yr}^{-1}$ , Midorikawa et al. (2012);  $-0.0043 \pm 0.0016$  to  $-0.0009 \pm 0.0007 \text{ pH}_T \text{ units yr}^{-1}$ , Leseurre et al. (2022)), these trends in the deep layer of the western basin are one order of magnitude higher than any area in the coastal zone and surrounding ocean. Additionally, the entire Southern Ocean exhibits a pH trend of  $-0.0020 \pm 0.0002 \text{ pH}_T \text{ units yr}^{-1}$  (Lauvset et al., 2015), similar to those surrounding the Antarctic Peninsula, but smaller than that estimated here in the western basin of the Bransfield Strait. Conversely, the central basin revealed interannual swinging but undefined trends (Table 2, Figure S11d in Supporting Information S1) over the 30 years investigated because of the dominance of DSW contributions. Furthermore, the intense well-mixed water column in the eastern basin may be the reason for the lower trend in the present study (Table 2, Figure S12 in Supporting Information S1).

Hence, we suggest that three possible processes may be driving  $\text{pH}_{\text{sws}}$  trends in the western basin: (a) intensified CDW intrusions over the continental shelf of the western basin and the NAP due to the increased frequency of years marked by the SAM+ phase (Henley et al., 2020; Jones et al., 2017); (b) transport of meltwater signals, via vertical mixing, throughout the water column with its carbon content (Monteiro, Kerr, Orselli, et al., 2020) during more intense wind-stress in SAM+ and ENSO- events; and (c) increased mixture between modified-CDW and DSW—while the former is rich in organic matter decomposition products, the latter is also enriched with anthropogenic carbon. The latter point is associated with its increased contribution to the Bransfield Strait in the 2010s

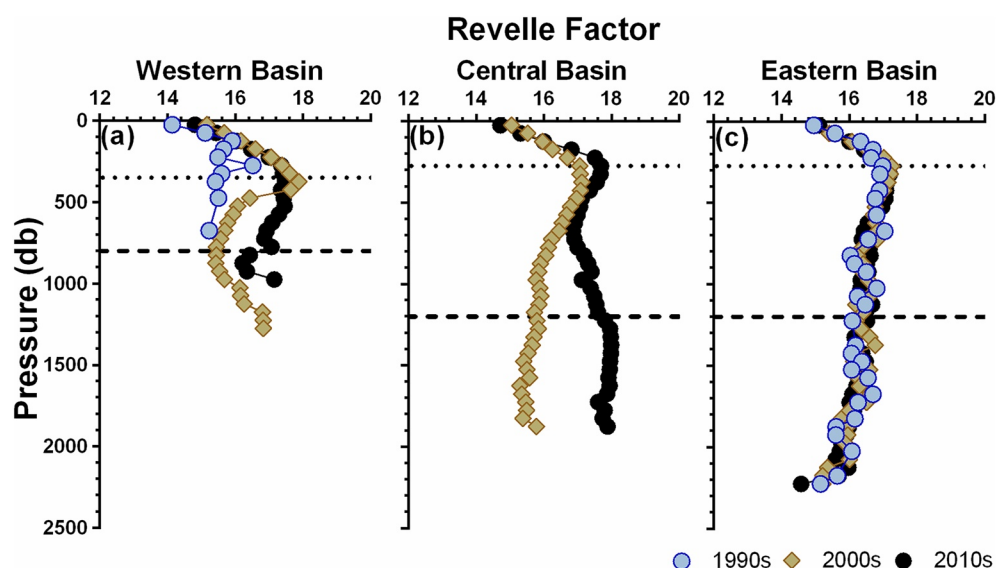


**Figure 6.** Vertical distribution of the Revelle factor over three decades in the Bransfield Strait for (a) western, (b) central, and (c) eastern basins. Plotted data is the average ( $\pm$ standard error) at each 50 m depth intervals. The black horizontal dotted and dashed lines in the panels represent the average value of the neutral density levels of 28.00 and 28.27 kg m<sup>-3</sup>, respectively.

(Damini et al., 2022; Dotto et al., 2016; Ruiz Barlett et al., 2018), which may yield the sharpest negative trends observed in the deep layer in the western basin as also noticed for the Gerlache Strait (Lencina-Avila et al., 2018). Indeed, the source area of DSW in the north-western Weddell Sea presented a reduction of 0.02 pH<sub>T</sub> units from 1992 to 2008 (Hauck et al., 2010), which may be carried into the Bransfield Strait. However, other processes take place in the water column, such as organic matter decomposition in the central basin (see Figures 5b and 5c), that may dampen this signature. However, since DSW is ventilated before flowing into the deepest layers of the Bransfield Strait (Dotto et al., 2016; van Caspel et al., 2018), the signature of atmospheric CO<sub>2</sub> increase may be absorbed by DSW (see Figure 5c).

Trends of pH<sub>sws</sub> respond to the CO<sub>2</sub> increment in the water column of the Bransfield Strait. This is corroborated by the decadal rising of the Revelle Factor for the western and central basins throughout the water column (Figures 6a and 6b), reaching values close to those observed in the eastern basin (Figure 6c). However, decadal changes in the central basin were more intense than those in the western basin because of the likely contribution of anthropogenic processes, such as the signature of atmospheric CO<sub>2</sub> increase due to the recent human footprint on the carbon cycle (i.e., anthropogenic carbon) in the Bransfield Strait. Since a high signature of modified-CDW is detected in the western basin, the decreases in pH<sub>sws</sub> in the region were related to the old and acidified water mass carrying natural products of organic matter decomposition. However, most frequent CDW intrusions respond to changes in modes of climate variability because of anthropogenic activities. Furthermore, the eastern basin has low influence of both water masses, reflecting a more mixed water mass structure in the region even with a Revelle Factor indicating that the basin has already been near CO<sub>2</sub> saturation since the 1990s (Figure 6c). Although this acidification process is minimal, the complexity of the eastern basin needs further investigation to clarify the reasons for its particular hydrographic and biogeochemical variability.

Overall, the Bransfield Strait demonstrated being close to reaching CO<sub>2</sub> saturation (i.e., reducing its capacity to store CO<sub>2</sub>). This condition implies that the acidification state in the strait is associated with a decrease in pH and saturation of calcium carbonate. For example, depths below 800 m in the 2010s are characterized by  $\Omega_{ar}$  with values below 1 (Figure 4e; i.e., undersaturated condition, prevailing dissolution over precipitation). It represents an issue for much more intense negative pH<sub>sws</sub> trends with impacts on calcified structures of marine organisms (i.e., decreasing  $\Omega$  values, mainly with respect to aragonite, the most unstable carbonate calcium



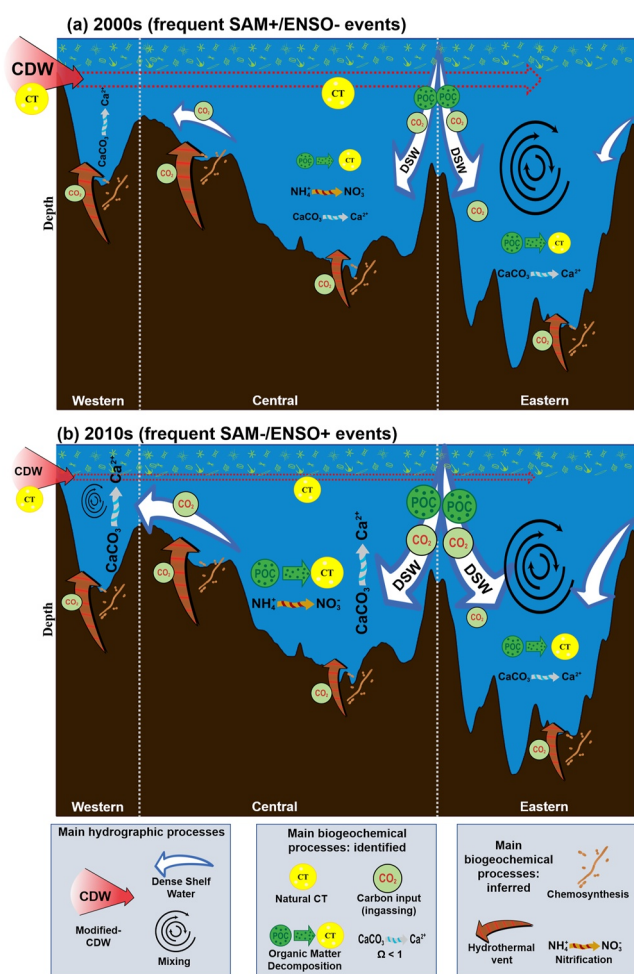


**Figure 7.** Conceptual model of the main processes affecting  $\text{CO}_2$ -carbonate system variability over three decades in the Bransfield Strait, northern Antarctic Peninsula. Panels present the state of the area in (a) the 2000s (prevailing SAM+ and ENSO-) and (b) the 2010s (prevailing SAM- and ENSO+). The highlighted section crosses from southeastern (left) to north-eastern (right). The red-dashed lines indicate bounds by sills between basins. The acronyms are as follows: CDW—Circumpolar Deep Water; CT—total inorganic carbon;  $\text{CO}_2$ —ingassing carbon dioxide; POC—particulate organic carbon;  $\text{CaCO}_3$ —calcium carbonate;  $\text{Ca}^{2+}$ —calcium ion;  $\text{NH}_4^+$ —ammonium ion; and  $\text{NO}_3^-$ —nitrate ion.

mineral) in the water column, such as pteropods, and on the seafloor, such as echinoderms and bryozoans (Acqua et al., 2019; Figuerola et al., 2020; Henley et al., 2020).

## 6. Conclusions

The changes in hydrography and climate modes variability (e.g., ENSO and SAM) that regulate ocean dynamics played key roles in altering marine carbonate chemistry in the Bransfield Strait. Periods of SAM+ intensified modified-CDW intrusions into the western basin during the 2000s, which is reflected in TA and CT dilution. This is mainly caused by meltwater inputs, as a consequence of the heat transported by CDW over the continental shelf of the western Antarctic Peninsula. This impact is followed by decreases in pH,  $\Omega_{\text{ar}}$  and  $\Omega_{\text{ca}}$  as an effect of the natural low pH of both CDW and melting water. On the other hand, the 2010s were characterized by intense DSW intrusions into the deep layers of the Bransfield Strait. DSW carries a signature of  $\text{CO}_2$  concentration from the north-western Weddell Sea, which is regulated by sea-air interactions and biological production. These processes intensified the CT positive trends over the last three decades. Also, the increased contribution of DSW into the western basin during the 2010s, for example, intensified the negative pH trends through mixing with modified-CDW intrusions. Conversely, the eastern basin exhibits a water mass structure driven by internal mixing, which minimizes any effect of water mass contribution and prevailing modes of climate variability.

It is important to highlight that biological (e.g., organic matter decomposition and nitrification) and other geochemical (e.g., hydrothermal vents as carbon inputs) processes may influence the carbonate system in the Bransfield Strait, but they require further investigation to determine their influence on TA and CT over time, and consequently on  $p\text{CO}_2$  and pH. Another substantial contribution to carbonate chemistry might come from anthropogenic carbon, which has been little investigated in the Bransfield Strait, masking its contribution to a region that is nearing  $\text{CO}_2$  saturation. A summary of identified and inferred hydrographic and biogeochemical processes of the 2000s and 2010s that can contribute to this variability in carbonate chemistry is provided (Figure 7).

The Bransfield Strait draws attention to the critical state of the influence of open ocean areas on coastal zones around the Antarctic Peninsula because it connects subpolar and polar systems. As part of the Southern Ocean, the Bransfield Strait draws attention to a countereffect of atmospheric  $\text{CO}_2$  increase because the region is experiencing a significant increase in sea surface temperature and is prone to reach  $\text{CO}_2$  saturation. The high Revelle Factor found here pinpoints the Bransfield Strait as a quasi-saturated region, which highlights a change toward a low capacity to absorb and store  $\text{CO}_2$ .

## Conflict of Interest

The authors declare no conflicts of interest relevant to this study.

## Data Availability Statement

Data from reconstructed parameters are available at <https://doi.org/10.5281/zenodo.7416652> (Santos-Andrade et al., 2022).



## Acknowledgments

This study is part of the activities of the Brazilian High Latitude Oceanography Group (GOAL) within the Brazilian Antarctic Program (PROANTAR). GOAL has been funded by and/or has received logistical support from the Brazilian Ministry of the Environment (MMA); the Brazilian Ministry of Science, Technology, and Innovation (MCTI); the Council for Research and Scientific Development of Brazil (CNPq); the Brazilian Navy; the Interministerial Secretariat for Sea Resources (SECIRM); the National Institute of Science and Technology of the Cryosphere (INCT CRIOSFERA; CNPq Grant 573720/2008-8 and 465680/2014-3); and the Research Support Foundation of the State of Rio Grande do Sul (FAPERGS Grant 17/2551-000518-0). This study was conducted within the activities of GOAL projects (CNPq Grant 550370/2002-1, 520189/2006-0, 556848/2009-8, 565040/2010-3, 405869/2013-4, 407889/2013-2, 442628/2018-8, and 442637/2018-7). Financial support was also received from the Coordination for the Improvement of Higher Education Personnel (CAPES) through the project CAPES “Ciências do Mar” (Grant 23038.001421/2014-30). CAPES also provided free access to many relevant journals through the portal “Periódicos CAPES” and the activities of the Graduate Program in Oceanology. Rodrigo Kerr and Mauricio M. Mata are granted with researcher fellowships from CNPq Grant 304937/2018-5 and 306896/2015-0, respectively. Mauricio Santos-Andrade acknowledges financial support from the CNPq scholarship Grant 132983/2020-6. The authors thank the officers and crew of the polar vessels Ary Rongel and Almirante Maximiano of the Brazilian Navy, and several scientists and technicians participating in the cruises, for their valuable help during data sampling and data processing. We thank all scientists and research groups for making their data available. All data sets used and their respective websites are indicated in the manuscript. We are grateful for the constructive comments provided by Elizabeth Jones, the Editors, and the anonymous reviewer, who helped to substantially improve the manuscript.

## References

- Abernathy, R. P., Ceroveck, I., Holland, P. R., Newsom, E., Mazloff, M., & Talley, L. D. (2016). Water-mass transformation by sea ice in the upper branch of the Southern Ocean overturning. *Nature Geoscience*, 9(8), 596–601. <https://doi.org/10.1038/ngeo2749>
- Acqua, O. D., Ferrando, S., Chiantore, M., & Asnaghi, V. (2019). The impact of ocean acidification on the gonads of three key Antarctic benthic macroinvertebrates. *Aquatic Toxicology*, 210, 19–29. <https://doi.org/10.1016/j.aquatox.2019.02.012>
- Almendros, J., Wilcock, W., Soule, D., Teixidó, T., Vizcaíno, L., Ardanaz, O., et al. (2020). BRAVOSEIS: Geophysical investigation of rift- and volcanism in the Bransfield strait, Antarctica. *Journal of South American Earth Sciences*, 104, 102834. <https://doi.org/10.1016/j.jsames.2020.102834>
- Alvarez, M., Aida, F. R., & Ros, G. (2002). Spatio-temporal variability of air-sea fluxes of carbon dioxide and oxygen in the Bransfield and Gerlache Straits during Austral summer 1995–96. *Deep-Sea Research Part II*, 49(4–5), 643–662. [https://doi.org/10.1016/S0967-0645\(01\)00116-3](https://doi.org/10.1016/S0967-0645(01)00116-3)
- Álvarez-Valero, A. M., Gisbert, G., Aulinas, M., Geyer, A., Kereszturi, G., Polo-Sánchez, A., et al. (2020).  $\delta D$  and  $\delta^{18}O$  variations of the magmatic system beneath Deception Island volcano (Antarctica): Implications for magma ascent and eruption forecasting. *Chemical Geology*, 542, 1–15. <https://doi.org/10.1016/j.chemgeo.2020.119595>
- Anadón, R., & Estrada, M. (2002). The FRUELA cruises. A carbon flux study in productive areas of the Antarctic Peninsula (December 1995–February 1996). *Deep-Sea Research Part II Topical Studies in Oceanography*, 49(4–5), 567–583. [https://doi.org/10.1016/S0967-0645\(01\)00112-6](https://doi.org/10.1016/S0967-0645(01)00112-6)
- Anderson, L. G., Holby, O., Lindegren, R., & Ohlson, M. (1991). The transport of anthropogenic carbon dioxide into the Weddell Sea. *Journal of Geophysical Research*, 96(C9), 16679. <https://doi.org/10.1029/91jc01785>
- Arrigo, K. R., Pabi, S., Van Dijken, G. L., & Maslowski, W. (2010). Air-sea flux of  $CO_2$  in the Arctic Ocean, 1998–2003. *Journal of Geophysical Research*, 115(4), 1998–2003. <https://doi.org/10.1029/2009JG001224>
- Avelina, R., da Cunha, L. C., Farias, C. D. O., Hamacher, C., Kerr, R., & Mata, M. M. (2020). Contrasting dissolved organic carbon concentrations in the Bransfield Strait, northern Antarctic Peninsula: Insights into ENSO and SAM effects. *Journal of Marine Systems*, 212, 103457. <https://doi.org/10.1016/j.jmarsys.2020.103457>
- Azaneu, M., Kerr, R., Mata, M. M., & Garcia, C. A. E. (2013). Trends in the deep Southern Ocean (1958–2010): Implications for Antarctic bottom water properties and volume export. *Journal of Geophysical Research: Oceans*, 118(9), 4213–4227. <https://doi.org/10.1002/jgrc.20303>
- Bittig, H. C., Steinhoff, T., Claustre, H., Fiedler, B., Williams, N. L., Sauzède, R., et al. (2018). An alternative to static climatologies: Robust estimation of open ocean  $CO_2$  variables and nutrient concentrations from T, S, and  $O_2$  data using Bayesian neural networks. *Frontiers in Marine Science*, 5, 1–29. <https://doi.org/10.3389/fmars.2018.00328>
- Blackford, J. C., & Gilbert, F. J. (2007). pH variability and  $CO_2$  induced acidification in the North Sea. *Journal of Marine Systems*, 64(1–4), 229–241. <https://doi.org/10.1016/j.jmarsys.2006.03.016>
- Boyer, T. P., Baranova, O. K., Coleman, C., Garcia, H. E., Grodsky, A., Locarnini, R. A., et al. (2018). NOAA atlas NESDIS 87. *World Ocean Database 2018*, 1–207.
- Broullón, D., Pérez, F. F., Velo, A., Hoppema, M., Olsen, A., Takahashi, T., et al. (2019). A global monthly climatology of total alkalinity: A neural network approach. *Earth System Science Data*, 11(3), 1109–1127. <https://doi.org/10.5194/essd-11-1109-2019>
- Broullón, D., Pérez, F. F., Velo, A., Hoppema, M., Olsen, A., Takahashi, T., et al. (2020). A global monthly climatology of oceanic total dissolved inorganic carbon: A neural network approach. *Earth System Science Data*, 12(3), 1725–1743. <https://doi.org/10.5194/essd-12-1725-2020>
- Brown, M. S., Munro, D. R., Feehan, C. J., Sweeney, C., Ducklow, H. W., & Schofield, O. M. (2019). Enhanced oceanic  $CO_2$  uptake along the rapidly changing West Antarctic Peninsula. *Nature Climate Change*, 9(9), 678–683. <https://doi.org/10.1038/s41558-019-0552-3>
- Carter, B. R., Feely, R. A., Williams, N. L., Dickson, A. G., Fong, M. B., & Takeshita, Y. (2018). Updated methods for global locally interpolated estimation of alkalinity, pH, and nitrate. *Limnology and Oceanography: Methods*, 16(2), 119–131. <https://doi.org/10.1002/lom3.10232>
- Castro, C. G., Ríos, A. F., Doval, M. D., & Pérez, F. F. (2002). Nutrient utilisation and chlorophyll distribution in the Atlantic sector of the Southern Ocean during Austral summer 1995–96. *Deep-Sea Research Part II Topical Studies in Oceanography*, 49(4–5), 623–641. [https://doi.org/10.1016/S0967-0645\(01\)00115-1](https://doi.org/10.1016/S0967-0645(01)00115-1)
- Clowes, A. J. (1934). Hydrology of the Bransfield Strait. In *Discovery reports* (pp. 1–64).
- Cook, A. J., Fox, A. J., Vaughan, D. G., & Ferrigno, J. G. (2005). Retreating glacier fronts on the Antarctic Peninsula over the past half-century. *Science*, 308(5721), 541–544. <https://doi.org/10.1126/science.1104235>
- Cook, A. J., Holland, P. R., Meredith, M. P., Murray, T., Luckman, A., & Vaughan, D. G. (2016). Ocean forcing of glacier retreat in the western Antarctic Peninsula. *Science*, 353(6296), 283–286. <https://doi.org/10.1126/science.aac0017>
- Costa, R. R., Mendes, C. R. B., Souza, M. S. D., Tavano, V. M., & Secchi, E. R. (2022). Chemotaxonomic characterization of the key genera of diatoms in the Northern Antarctic Peninsula. *Anais da Academia Brasileira de Ciências*, 94, e20210584. <https://doi.org/10.1590/0001-376520220210584>
- Costa, R. R., Mendes, C. R. B., Tavano, V. M., Dotto, T. S., Kerr, R., Monteiro, T., et al. (2020). Dynamics of an intense diatom bloom in the northern Antarctic Peninsula, February 2016. *Limnology and Oceanography*, 65(9), 1–20. <https://doi.org/10.1002/lno.11437>
- Damini, B. Y., Costa, R. R., Dotto, T. S., Rafael, C., Mendes, B., Torres-Iasso, J. C., et al. (2023). Antarctica Slope Front bifurcation eddy: A stationary feature influencing  $CO_2$  dynamics in the northern Antarctic Peninsula. *Progress in Oceanography*, 212, 102985. <https://doi.org/10.1016/j.pocan.2023.102985>
- Damini, B. Y., Kerr, R., Dotto, T. S., & Mata, M. M. (2022). Long-term changes on the Bransfield Strait deep water masses: Variability, drivers and connections with the northwestern Weddell Sea. *Deep Sea Research Part I: Oceanographic Research Papers*, 179, 103667. <https://doi.org/10.1016/j.dsr.2021.103667>
- De Lavergne, C., Palter, J. B., Galbraith, E. D., Bernardello, R., & Marinov, I. (2014). Cessation of deep convection in the open Southern Ocean under anthropogenic climate change. *Nature Climate Change*, 4(4), 278–282. <https://doi.org/10.1038/nclimate2132>
- Detoni, A. M. S., de Souza, M. S., Garcia, C. A. E., Tavano, V. M., & Mata, M. M. (2015). Environmental conditions during phytoplankton blooms in the vicinity of James Ross Island, east of the Antarctic Peninsula. *Polar Biology*, 38(8), 1111–1127. <https://doi.org/10.1007/s00300-015-1670-7>
- Dickson, A. G. (1990). Thermodynamics of the dissociation of boric acid in potassium chloride solutions from 273.15 to 318.15 K. *Journal of Chemical and Engineering Data*, 35(3), 253–257. <https://doi.org/10.1021/jc00061a009>
- Dickson, A. G., Dickson, A. G., Afghan, J. D., & Anderson, G. C. (2003). Reference materials for oceanic  $CO_2$  analysis: A method for the certification of total alkalinity. *Marine Chemistry*, 80(2–3), 185–197. [https://doi.org/10.1016/S0304-4203\(02\)00133-0](https://doi.org/10.1016/S0304-4203(02)00133-0)
- Dinniman, M. S., Klinck, J. M., & Hofmann, E. E. (2012). Sensitivity of circumpolar deep water transport and ice shelf basal melt along the west Antarctic Peninsula to changes in the winds. *Journal of Climate*, 25(14), 4799–4816. <https://doi.org/10.1175/JCLI-D-11-00307.1>

- Dinniman, M. S., Klinck, J. M., & Smith, W. O. (2011). A model study of circumpolar deep water on the west Antarctic Peninsula and Ross Sea continental shelves. *Deep-Sea Research Part II Topical Studies in Oceanography*, 58(13–16), 1508–1523. <https://doi.org/10.1016/j.dsr2.2010.11.013>
- Dotto, T. S., Kerr, R., Mata, M. M., & Garcia, C. A. E. (2016). Multidecadal freshening and lightening in the deep waters of the Bransfield Strait, Antarctica. *Journal of Geophysical Research: Oceans*, 121(6), 3741–3756. <https://doi.org/10.1002/2015JC011228>
- Dotto, T. S., Mata, M. M., Kerr, R., & Garcia, C. A. E. (2021). A novel hydrographic gridded data set for the northern Antarctic Peninsula. *Earth System Science Data*, 13(2), 671–696. <https://doi.org/10.5194/essd-13-671-2021>
- Doval, M. D., Álvarez-Salgado, X. A., Castro, C. G., & Pérez, F. F. (2002). Dissolved organic carbon distributions in the Bransfield and Gerlache Straits, Antarctica. *Deep-Sea Research Part II Topical Studies in Oceanography*, 49(4–5), 663–674. [https://doi.org/10.1016/S0967-0645\(01\)00117-5](https://doi.org/10.1016/S0967-0645(01)00117-5)
- Figuerola, B., Hancock, A. M., Bax, N., Cummings, V., Downey, R., Griffiths, H. J., et al. (2020). Predicting potential impacts of ocean acidification on marine calcifiers from the Southern Ocean, (Lmc), (pp. 1–36). <https://doi.org/10.1101/2020.11.15.384131>
- Figuerola, B., Hancock, A. M., Bax, N., Cummings, V. J., Downey, R., Griffiths, H. J., et al. (2021). A review and meta-analysis of potential impacts of ocean acidification on marine calcifiers from the Southern Ocean. *Frontiers in Marine Science*, 8, 584445. <https://doi.org/10.3389/fmars.2021.584445>
- Fischer, G. (1991). Stable carbon isotope ratios of plankton carbon and sinking organic matter from the Atlantic sector of the Southern Ocean. *Marine Chemistry*, 35(1–4), 581–596. [https://doi.org/10.1016/S0304-4203\(09\)90044-5](https://doi.org/10.1016/S0304-4203(09)90044-5)
- Fisk, M. R. (1990). Volcanism in the Bransfield Strait, Antarctica. *Journal of South American Earth Sciences*, 3(2–3), 91–101. [https://doi.org/10.1016/0895-9811\(90\)90022-S](https://doi.org/10.1016/0895-9811(90)90022-S)
- Fofonoff, N. P., & Millard, R. C. (1983). Algorithms for computation of fundamental properties of seawater. *UNESCO Technical Papers in Marine Science*, 44, 1–53.
- Frölicher, T. L., Sarmiento, J. L., Paynter, D. J., Dunne, J. P., Krasting, J. P., & Winton, M. (2015). Dominance of the Southern Ocean in anthropogenic carbon and heat uptake in CMIP5 models. *Journal of Climate*, 28(2), 862–886. <https://doi.org/10.1175/JCLI-D-14-00117.1>
- García, M. A., Castro, C. G., Ríos, A. F., Doval, M. D., Rosón, G., Gomis, D., & López, O. (2002). Water masses and distribution of physico-chemical properties in the Western Bransfield Strait and Gerlache Strait during austral summer 1995/96. *Deep-Sea Research Part II Topical Studies in Oceanography*, 49(4–5), 585–602. [https://doi.org/10.1016/S0967-0645\(01\)00113-8](https://doi.org/10.1016/S0967-0645(01)00113-8)
- Gille, S. T. (2008). Decadal-scale temperature trends in the Southern Hemisphere ocean. *Journal of Climate*, 21(18), 4749–4765. <https://doi.org/10.1175/2008JCLI2131.1>
- Gordon, A. L., Mensch, M., Dong, Z., Smethie, W. M., & De Bettencourt, J. (2000). Deep and bottom water of the Bransfield Strait eastern and central basins. *Journal of Geophysical Research*, 105(C5), 11337–11346. <https://doi.org/10.1029/2000jc900030>
- Goyet, C., & Davis, D. (1997). Estimation of total CO<sub>2</sub> concentration throughout the water column. *Deep Sea Research Part I: Oceanographic Research Papers*, 44(5), 859–877. [https://doi.org/10.1016/S0967-0637\(96\)00111-2](https://doi.org/10.1016/S0967-0637(96)00111-2)
- Goyet, C., & Poisson, A. (1989). New determination of carbonic acid dissociation constants in seawater as a function of temperature and salinity. *Deep-Sea Research, Part A: Oceanographic Research Papers*, 36(11), 1635–1654. [https://doi.org/10.1016/0198-0149\(89\)90064-2](https://doi.org/10.1016/0198-0149(89)90064-2)
- Hauck, J., Hoppema, M., Bellerby, R. G. J., Völker, C., & Wolf-Gladrow, D. (2010). Data-based estimation of anthropogenic carbon and acidification in the Weddell Sea on a decadal timescale. *Journal of Geophysical Research*, 115(3), 1–14. <https://doi.org/10.1029/2009JC005479>
- Haumann, F. A., Gruber, N., Münnich, M., Frenger, I., Kern, S., Alexander Haumann, F., et al. (2016). Sea-ice transport driving Southern Ocean salinity and its recent trends. *Nature*, 537(7618), 89–92. <https://doi.org/10.1038/nature19101>
- Hauri, C., Doney, S. C., Takahashi, T., Erickson, M., Jiang, G., & Ducklow, H. W. (2015). Two decades of inorganic carbon dynamics along the West Antarctic Peninsula. *Biogeosciences*, 12(22), 6761–6779. <https://doi.org/10.5194/bg-12-6761-2015>
- Hellmer, H. H., Huhn, O., Gomis, D., & Timmermann, R. (2011). On the freshening of the northwestern Weddell Sea continental shelf. *Ocean Science*, 7(3), 305–316. <https://doi.org/10.5194/os-7-305-2011>
- Hellmer, H. H., Kauker, F., Timmermann, R., & Hattermann, T. (2017). The fate of the Southern Weddell Sea continental shelf in a warming climate. *Journal of Climate*, 30(12), 4337–4350. <https://doi.org/10.1175/JCLI-D-16-0420.1>
- Henley, S. F., Cavan, E. L., Fawcett, S. E., Kerr, R., Monteiro, T., Sherrell, R. M., et al. (2020). Changing biogeochemistry of the Southern Ocean and its ecosystem implications. *Frontiers in Marine Science*, 7, 1–31. <https://doi.org/10.3389/fmars.2020.00581>
- Henley, S. F., Schofield, O. M., Hendry, K. R., Schloss, I. R., Steinberg, D. K., Moffat, C., et al. (2019). Variability and change in the west Antarctic Peninsula marine system: Research priorities and opportunities. *Progress in Oceanography*, 173, 208–237. <https://doi.org/10.1016/j.pcean.2019.03.003>
- Hofmann, E. E., Klinck, J. M., Lascara, C. M., & Smith, D. A. (1996). Water mass distribution and circulation west of the Antarctic Peninsula and including Bransfield Strait. In *Foundations for ecological research west of the Antarctic Peninsula: Antarctic research series* (pp. 61–80). <https://doi.org/10.1029/AR070p0061>
- Hunke, W. G. C., Huhn, O., & Schröder, M. (2016). Water masses in the Bransfield Strait and adjacent seas, austral summer 2013. *Polar Biology*, 39(5), 789–798. <https://doi.org/10.1007/s00300-016-1936-8>
- Ito, R. G., Tavano, V. M., Mendes, C. R. B., & Garcia, C. A. E. (2018). Sea-air CO<sub>2</sub> fluxes and pCO<sub>2</sub> variability in the Northern Antarctic Peninsula during three summer periods (2008–2010). *Deep-Sea Research Part II Topical Studies in Oceanography*, 149, 84–98. <https://doi.org/10.1016/j.dsr2.2017.09.004>
- Jiang, L. Q., Carter, B. R., Feely, R. A., Lauvset, S. K., & Olsen, A. (2019). Surface ocean pH and buffer capacity: Past, present and future. *Scientific Reports*, 9(1), 1–11. <https://doi.org/10.1038/s41598-019-55039-4>
- Jones, E. M., Fenton, M., Meredith, M. P., Clargo, N. M., Ossebaar, S., Ducklow, H. W., et al. (2017). Ocean acidification and calcium carbonate saturation states in the coastal zone of the West Antarctic Peninsula. *Deep-Sea Research Part II Topical Studies in Oceanography*, 139, 181–194. <https://doi.org/10.1016/j.dsr2.2017.01.007>
- Karl, D. M., Tilbrook, B., & Tien, G. (1990). Seasonal coupling of organic matter production and particle flux in the western Bransfield Strait, Antarctica. *Deep-Sea Research*, 38(8–9), 1097–1126. [https://doi.org/10.1016/0198-0149\(91\)90098-z](https://doi.org/10.1016/0198-0149(91)90098-z)
- Kerr, R., Goyet, C., da Cunha, L. C., Orselli, I. B. M., Lencina-Avila, J. M., Mendes, C. R. B., et al. (2018). Carbonate system properties in the Gerlache Strait, northern Antarctic Peninsula (February 2015): II. Anthropogenic CO<sub>2</sub> and seawater acidification. *Deep-Sea Research Part II Topical Studies in Oceanography*, 149, 182–192. <https://doi.org/10.1016/j.dsr2.2017.07.007>
- Kerr, R., Mata, M. M., Mendes, C. R. B., & Secchi, E. R. (2018). Northern Antarctic Peninsula: A marine climate hotspot of rapid changes on ecosystems and ocean dynamics. *Deep-Sea Research Part II Topical Studies in Oceanography*, 149, 4–9. <https://doi.org/10.1016/j.dsr2.2018.05.006>

- Kerr, R., Orselli, I. B. M., Lencina-Avila, J. M., Eidt, R. T., Mendes, C. R. B., da Cunha, L. C., et al. (2018). Carbonate system properties in the Gerlache Strait, northern Antarctic Peninsula (February 2015): I. Sea–Air CO<sub>2</sub> fluxes. *Deep-Sea Research Part II Topical Studies in Oceanography*, 149, 171–181. <https://doi.org/10.1016/j.dsr2.2017.02.008>
- Laika, H. E., Goyet, C., Voue, F., Poisson, A., & Touratier, F. (2009). Interannual properties of the CO<sub>2</sub> system in the Southern Ocean south of Australia. *Antarctic Science*, 21(6), 663–680. <https://doi.org/10.1017/S0954102009990319>
- Lauvset, S. K., Gruber, N., Landschützer, P., Olsen, A., & Tjiputra, J. (2015). Trends and drivers in global surface ocean pH over the past 3 decades. *Biogeosciences*, 12(5), 1285–1298. <https://doi.org/10.5194/bg-12-1285-2015>
- Lee, K., Tong, L. T., Millero, F. J., Sabine, C. L., Dickson, A. G., Goyet, C., et al. (2006). Global relationships of total alkalinity with salinity and temperature in surface waters of the world's oceans. *Geophysical Research Letters*, 33(19), L19605. <https://doi.org/10.1029/2006GL027207>
- Legge, O. J., Bakker, D. C. E., Meredith, M. P., Venables, H. J., Brown, P. J., Jones, E. M., & Johnson, M. T. (2017). The seasonal cycle of carbonate system processes in Ryder Bay, West Antarctic Peninsula. *Deep Sea Research Part II: Topical Studies in Oceanography*, 139, 167–180. <https://doi.org/10.1016/j.dsr2.2016.11.006>
- Lencina-Avila, J. M., Goyet, C., Kerr, R., Orselli, I. B. M., Mata, M. M., & Touratier, F. (2018). Past and future evolution of the marine carbonate system in a coastal zone of the Northern Antarctic Peninsula. *Deep-Sea Research Part II Topical Studies in Oceanography*, 149, 193–205. <https://doi.org/10.1016/j.dsr2.2017.10.018>
- Leseurre, C., Lo Monaco, C., Reverdin, G., Metzl, N., Fin, J., Mignon, C., & Benito, L. (2022). Trends and drivers of sea surface fCO<sub>2</sub> and pH changes observed in Southern Indian Ocean over the last two decades. *Biogeosciences*, 19(10), 2599–2625. <https://doi.org/10.5194/bg-2022-22>
- Lewis, E., & Wallace, D. (1998). *Program developed for CO<sub>2</sub> system calculations*. Ornl/Cdiac-105. Oak Ridge, Tenn: Carbon Dioxide Information Analysis Center. Retrieved from <http://cdiac.esd.ornl.gov/oceans/co2rprtnbk.html>
- Loeb, V. J., Hofmann, E. E., Klinck, J. M., Holm-Hansen, O., & White, W. B. (2009). ENSO and variability of the Antarctic Peninsula pelagic marine ecosystem. *Antarctic Science*, 21(2), 135–148. <https://doi.org/10.1017/S0954102008001636>
- Lopez, O., Garcia, M. A., Gomis, D., Rojas, P., Sospedra, J., & Arcilla-Sánchez, A. (1999). Hydrographic and hydrodynamic characteristics of the eastern basin of the Bransfield Strait. *Deep Sea Research Part I: Oceanographic Research Papers*, 46(10), 1755–1778. [https://doi.org/10.1016/S0967-0637\(99\)00017-5](https://doi.org/10.1016/S0967-0637(99)00017-5)
- Marshall, G. J., Orr, A., van Lipzig, N. P. M., & King, J. C. (2006). The impact of a changing southern hemisphere annular mode on Antarctic Peninsula summer temperatures. *Journal of Climate*, 19(20), 5388–5404. <https://doi.org/10.1175/JCLI3844.1>
- Masqué, P., Isla, E., Sanchez-Cabeza, J. A., Palanques, A., Bruach, J. M., Puig, P., & Guillén, J. (2002). Sediment accumulation rates and carbon fluxes to bottom sediments at the western Bransfield Strait (Antarctica). *Deep-Sea Research Part II Topical Studies in Oceanography*, 49(4–5), 921–933. [https://doi.org/10.1016/S0967-0645\(01\)00131-X](https://doi.org/10.1016/S0967-0645(01)00131-X)
- Massom, R. A., Scambos, T. A., Bennetts, L. G., Reid, P., Squire, V. A., & Stammerjohn, S. E. (2018). Antarctic ice shelf disintegration triggered by sea ice loss and ocean swell. *Nature*, 558(7710), 383–389. <https://doi.org/10.1038/s41586-018-0212-1>
- Mata, M. M., & Garcia, C. A. E. (2016a). Physical oceanography during Ary Rongel cruise GOAL2003. <https://doi.org/10.1594/PANGAEA.863598>
- Mata, M. M., & Garcia, C. A. E. (2016b). Physical oceanography during Ary Rongel cruise GOAL2004. <https://doi.org/10.1594/PANGAEA.863599>
- Mata, M. M., & Garcia, C. A. E. (2016c). Physical oceanography during Ary Rongel cruise GOAL2005. <https://doi.org/10.1594/PANGAEA.863600>
- Mata, M. M., & Garcia, C. A. E. (2016d). Physical oceanography during Ary Rongel cruise SOS-climate I. <https://doi.org/10.1594/PANGAEA.864576>
- Mata, M. M., & Garcia, C. A. E. (2016e). Physical oceanography during Ary Rongel cruise SOS-climate II. <https://doi.org/10.1594/PANGAEA.864578>
- Mata, M. M., & Garcia, C. A. E. (2016f). Physical oceanography during Ary Rongel cruise SOS-climate III. <https://doi.org/10.1594/PANGAEA.864579>
- Mata, M. M., & Kerr, R. (2016a). Physical oceanography during Almirante Maximiano cruise POLARCANION-II. <https://doi.org/10.1594/PANGAEA.864592>
- Mata, M. M., & Kerr, R. (2016b). Physical oceanography during Almirante Maximiano cruise POLARCANION-III. <https://doi.org/10.1594/PANGAEA.864593>
- Mata, M. M., & Kerr, R. (2016c). Physical oceanography during Ary Rongel cruise POLARCANION-I. <https://doi.org/10.1594/PANGAEA.864591>
- Mata, M. M., Tavano, V. M., & Garcia, C. A. E. (2018). 15 years sailing with the Brazilian high latitude oceanography group (GOAL). *Deep-Sea Research Part II Topical Studies in Oceanography*, 149, 1–3. <https://doi.org/10.1016/j.dsr2.2018.05.007>
- McNeil, B. I., & Matear, R. J. (2008). Southern Ocean acidification: A tipping point at 450-ppm atmospheric CO<sub>2</sub>. *Proceedings of the National Academy of Sciences of the United States of America*, 105(48), 18860–18864. <https://doi.org/10.1073/pnas.0806318105>
- Mendes, C. R. B., Costa, R. R., Ferreira, A., Jesus, B., Tavano, V. M., Dotto, T. S., et al. (2023). Cryptophytes: An emerging algal group in the rapidly changing Antarctic Peninsula marine environments. *Global Change Biology*. <https://doi.org/10.1111/gcb.16602>
- Mendes, C. R. B., de Souza, M. S., Garcia, V. M. T., Leal, M. C., Brotas, V., & Garcia, C. A. E. (2012). Dynamics of phytoplankton communities during late summer around the tip of the Antarctic Peninsula. *Deep-Sea Research Part I Oceanographic Research Papers*, 65, 1–14. <https://doi.org/10.1016/j.dsr.2012.03.002>
- Meredith, M. P., Brandon, M. A., Wallace, M. I., Clarke, A., Leng, M. J., Renfrew, I. A., et al. (2008). Variability in the freshwater balance of northern Marguerite Bay, Antarctic Peninsula: Results from δ<sup>18</sup>O. *Deep-Sea Research Part II Topical Studies in Oceanography*, 55(3–4), 309–322. <https://doi.org/10.1016/j.dsr2.2007.11.005>
- Meredith, M. P., Jullion, L., Brown, P. J., Garabato, A. C. N., & Coudrey, M. P. (2014). Dense waters of the Weddell and Scotia seas: Recent changes in properties and circulation. *Philosophical Transactions of the Royal Society A: Mathematical, Physical & Engineering Sciences*, 372(2019), 1–11. <https://doi.org/10.1098/rsta.2013.0041>
- Meredith, M. P., & King, J. C. (2005). Rapid climate change in the ocean west of the Antarctic Peninsula during the second half of the 20th century. *Geophysical Research Letters*, 32(19), 1–5. <https://doi.org/10.1029/2005GL024042>
- Midorikawa, T., Inoue, H. Y., Ishii, M., Sasano, D., Kosugi, N., Hashida, G., et al. (2012). Decreasing pH trend estimated from 35-year time series of carbonate parameters in the Pacific sector of the Southern Ocean in summer. *Deep-Sea Research Part I Oceanographic Research Papers*, 61, 131–139. <https://doi.org/10.1016/j.dsr.2011.12.003>
- Millero, F. J. (2007). The marine inorganic carbon cycle. *Chemical Reviews*, 107(2), 308–341. <https://doi.org/10.1021/cr0503557>
- Millero, F. J., Lee, K., & Roche, M. (1998). Distribution of alkalinity in the surface waters of the major oceans. *Marine Chemistry*, 60(1–2), 111–130. [https://doi.org/10.1016/S0304-4203\(97\)00084-4](https://doi.org/10.1016/S0304-4203(97)00084-4)
- Moffat, C., & Meredith, M. (2018). Shelf-ocean exchange and hydrography west of the Antarctic Peninsula: A review. *Philosophical Transactions of the Royal Society A: Mathematical, Physical & Engineering Sciences*, 376(2122), 20170164. <https://doi.org/10.1098/rsta.2017.0164>
- Moffat, C., Owens, B., & Beardsley, R. C. (2009). On the characteristics of circumpolar deep water intrusions to the west Antarctic Peninsula continental shelf. *Journal of Geophysical Research*, 114(5), 1–16. <https://doi.org/10.1029/2008JC004955>



- Monteiro, T., Kerr, R., & Machado, E. D. C. (2020). Seasonal variability of net sea-air CO<sub>2</sub> fluxes in a coastal region of the northern Antarctic Peninsula. *Scientific Reports*, 10(1), 14875. <https://doi.org/10.1038/s41598-020-71814-0>
- Monteiro, T., Kerr, R., Orselli, I. B. M., & Lencina-Avila, J. M. (2020). Towards an intensified summer CO<sub>2</sub> sink behaviour in the Southern Ocean coastal regions. *Progress in Oceanography*, 183, 1–13. <https://doi.org/10.1016/j.poccean.2020.102267>
- Newton, J. A., Feely, R. A., Jewett, E. B., Williamson, P., & Mathis, J. (2015). Global Ocean acidification observing network: Requirements and governance plan. *Global ocean acidification observing network*, 5–28. Retrieved from [www.iaea.org/ocean-acidification](http://www.iaea.org/ocean-acidification)
- Nicholls, K. W., Østerhus, S., Makinson, K., Gammelsrød, T., & Fahrbach, E. (2009). Ice-ocean processes over the continental shelf of the southern Weddell Sea, Antarctica: A review. *Reviews of Geophysics*, 47(3), 1–23. <https://doi.org/10.1029/2007RG000250>
- Orr, J. C., Epitalon, J. M., Dickson, A. G., & Gattuso, J. P. (2018). Routine uncertainty propagation for the marine carbon dioxide system. *Marine Chemistry*, 207, 84–107. <https://doi.org/10.1016/j.marchem.2018.10.006>
- Orr, J. C., Fabry, V. J., Aumont, O., Bopp, L., Doney, S. C., Feely, R. A., et al. (2005). Anthropogenic ocean acidification over the twenty-first century and its impact on calcifying organisms. *Nature*, 437(7059), 681–686. <https://doi.org/10.1038/nature04095>
- Orselli, I. B. M., Carvalho, A. C. O., Monteiro, T., Damini, B. Y., Carvalho-Borges, M. D. E., Albuquerque, C., & Kerr, R. (2022). The marine carbonate system along the northern Antarctic Peninsula: Current knowledge and future perspectives. *Anais da Academia Brasileira de Ciências*, 94. <https://doi.org/10.1590/0001-376520220210825>
- Orselli, I. B. M., Kerr, R., Azevedo, J. L. L. D., Galdino, F., Araujo, M., & Garcia, C. A. E. (2019). Progress in oceanography the sea-air CO<sub>2</sub> net fluxes in the South Atlantic Ocean and the role played by Agulhas eddies. *Progress in Oceanography*, 170, 40–52. <https://doi.org/10.1016/j.poccean.2018.10.006>
- Pardo, P. C., Pérez, F. F., Khatiwala, S., & Ríos, A. F. (2014). Anthropogenic CO<sub>2</sub> estimates in the Southern Ocean: Storage partitioning in the different water masses. *Progress in Oceanography*, 120, 230–242. <https://doi.org/10.1016/j.poccean.2013.09.005>
- Perez, F. F., & Fraga, F. (1987). Association constant of fluoride and hydrogen ions in seawater. *Marine Chemistry*, 21(2), 161–168. [https://doi.org/10.1016/0304-4203\(87\)90036-3](https://doi.org/10.1016/0304-4203(87)90036-3)
- Reid, P. A., & Massom, R. A. (2022). Change and variability in Antarctic coastal exposure, 1979–2020. *Nature Communications*, 13(1164), 1–11. <https://doi.org/10.1038/s41467-022-28676-z>
- Renner, A. H. H., Thorpe, S. E., Heywood, K. J., Murphy, E. J., Watkins, J. L., & Meredith, M. P. (2012). Advective pathways near the tip of the Antarctic Peninsula: Trends, variability and ecosystem implications. *Deep-Sea Research Part I Oceanographic Research Papers*, 63, 91–101. <https://doi.org/10.1016/j.dsr.2012.01.009>
- Rignot, E., Mouginot, J., Scheuchl, B., Van Den Broeke, M., Van Wessem, M. J., & Morlighem, M. (2019). Four decades of Antarctic ice sheet mass balance from 1979–2017. *Proceedings of the National Academy of Sciences of the United States of America*, 116(4), 1095–1103. <https://doi.org/10.1073/pnas.1812883116>
- Rivaro, P., Messa, R., Ianni, C., Magi, E., & Budillon, G. (2014). Distribution of total alkalinity and pH in the Ross Sea (Antarctica) waters during austral summer 2008. *Polar Research*, 33(2014), 20403. <https://doi.org/10.3402/polar.v33.20403>
- Roden, N. P., Shadwick, E. H., Tilbrook, B., & Trull, T. W. (2013). Annual cycle of carbonate chemistry and decadal change in coastal. *Marine Chemistry*, 155, 135–147. <https://doi.org/10.1016/j.marchem.2013.06.006>
- Ruiz Barlett, E. M., Tosonotto, G. V., Piola, A. R., Sierra, M. E., & Mata, M. M. (2018). On the temporal variability of intermediate and deep waters in the Western Basin of the Bransfield Strait. *Deep-Sea Research Part II Topical Studies in Oceanography*, 149, 31–46. <https://doi.org/10.1016/j.dsr2.2017.12.010>
- Sabine, C. L., Feely, R. A., Gruber, N., Key, R. M., Lee, K., Bullister, J. L., et al. (2004). The oceanic sink for anthropogenic CO<sub>2</sub>. *Science*, 305(5682), 367–371. <https://doi.org/10.1126/science.1097403>
- Sabine, C. L., Feely, R. A., Millero, F. J., Dickson, A. G., Langdon, C., Mecking, S., & Greeley, D. (2008). Decadal changes in Pacific carbon. *Journal of Geophysical Research*, 113(7), 1–12. <https://doi.org/10.1029/2007JC004577>
- Sandrini, S., Ait-Ameur, N., Rivaro, P., Massolo, S., Touratier, F., Tositti, L., & Goyet, C. (2007). Anthropogenic carbon distribution in the Ross sea, Antarctica. *Antarctic Science*, 19(3), 395–407. <https://doi.org/10.1017/S0954102007000405>
- Sangrà, P., Gordo, C., Hernández-Arencibia, M., Marrero-Díaz, A., Rodríguez-Santana, A., Stegner, A., et al. (2011). The Bransfield current system. *Deep-Sea Research Part I Oceanographic Research Papers*, 58(4), 390–402. <https://doi.org/10.1016/j.dsr.2011.01.011>
- Sangrà, P., Stegner, A., Hernández-Arencibia, M., Marrero-Díaz, Á., Salinas, C., Aguiar-González, B., et al. (2017). The Bransfield gravity current. *Deep-Sea Research Part I Oceanographic Research Papers*, 119, 1–15. <https://doi.org/10.1016/j.dsr.2016.11.003>
- Santos-Andrade, M., Kerr, R., Orselli, I., Monteiro, T., Mata, M., & Goyet, C. (2022). Reconstructed carbonate system in the Bransfield Strait over the last 30 years (pp. 1990–2019). <https://doi.org/10.5281/zenodo.7416652>
- Scambos, T. A., Hulbe, C., Fahnestock, M., & Bohlander, J. (2000). The link between climate warming and break-up of ice shelves in the Antarctic Peninsula. *Journal of Glaciology*, 46(154), 516–530. <https://doi.org/10.3189/172756500781833043>
- Shepherd, A., Ivins, E., Rignot, E., Smith, B., van den Broeke, M., Velicogna, I., et al. (2018). Mass balance of the Antarctic Ice Sheet from 1992 to 2017. *Nature*, 558(7709), 219–222. <https://doi.org/10.1038/s41586-018-0179-y>
- Shepherd, A., Wingham, D., & Rignot, E. (2004). Warm ocean is eroding west Antarctic Ice Sheet. *Geophysical Research Letters*, 31(23), 1–4. <https://doi.org/10.1029/2004GL021106>
- Siebert, M., Atkinson, A., Banwell, A., Brandon, M., Convey, P., Davies, B., et al. (2019). The Antarctic Peninsula under a 1.5°C global warming scenario. *Frontiers in Environmental Science*, 7, 1–7. <https://doi.org/10.3389/fenvs.2019.00102>
- Signori, C. N., Thomas, F., Enrich-Prast, A., Pollery, R. C. G., & Sievert, S. M. (2014). Microbial diversity and community structure across environmental gradients in Bransfield Strait, Western Antarctic Peninsula. *Frontiers in Microbiology*, 5, 1–12. <https://doi.org/10.3389/fmicb.2014.00647>
- Takahashi, T., Sutherland, S. C., Chipman, D. W., Goddard, J. G., Ho, C., Newberger, T., et al. (2014). Climatological distributions of pH, pCO<sub>2</sub>, total CO<sub>2</sub>, alkalinity, and CaCO<sub>3</sub> saturation in the global surface ocean, and temporal changes at selected locations. *Marine Chemistry*, 164, 95–125. <https://doi.org/10.1016/j.marchem.2014.06.004>
- Turner, S., Tonarini, S., Bindeman, I., Leeman, W. P., & Schaefer, B. F. (2007). Boron and oxygen isotope evidence for recycling of subducted components over the past 2.5 Gyr. *Nature*, 447(7145), 702–705. <https://doi.org/10.1038/nature05898>
- Uppström, L. R. (1974). The boron/chlorinity ratio of deep-sea water from the Pacific Ocean. *Deep-Sea Research and Oceanographic Abstracts*, 21(2), 161–162. [https://doi.org/10.1016/0011-7471\(74\)90074-6](https://doi.org/10.1016/0011-7471(74)90074-6)
- van Cappel, M., Hellmer, H. H., & Mata, M. M. (2018). On the ventilation of Bransfield Strait deep basins. *Deep-Sea Research Part II Topical Studies in Oceanography*, 149, 25–30. <https://doi.org/10.1016/j.dsr2.2017.09.006>
- van Heuven, S. M. A. C., Hoppema, M., Jones, E. M., & de Baar, H. J. W. (2014). Rapid invasion of anthropogenic CO<sub>2</sub> into the deep circulation of the Weddell Gyre. *Philosophical Transactions of the Royal Society A: Mathematical, Physical & Engineering Sciences*, 372(2019), 1–11. <https://doi.org/10.1098/rsta.2013.0056>

- Von Gylidenfeldt, A. B., Fahrbach, E., García, M. A., & Schröder, M. (2002). Flow variability at the tip of the Antarctic Peninsula. *Deep-Sea Research Part II Topical Studies in Oceanography*, 49(21), 4743–4766. [https://doi.org/10.1016/S0967-0645\(02\)00157-1](https://doi.org/10.1016/S0967-0645(02)00157-1)
- Wang, X., Moffat, C., Dinniman, M. S., Klinck, J. M., Sutherland, D. A., & Aguiar-González, B. (2022). Variability and dynamics of along-shore exchange on the west Antarctic Peninsula (WAP) continental shelf. *Journal of Geophysical Research: Oceans*, 127(2), e2021JC017645. <https://doi.org/10.1029/2021JC017645>
- Wanninkhof, R., Lewis, E., Feely, R. A., & Millero, F. J. (1999). The optimal carbonate dissociation constants for determining surface water pCO<sub>2</sub> from alkalinity and total inorganic carbon. *Marine Chemistry*, 65(3–4), 291–301. [https://doi.org/10.1016/S0304-4203\(99\)00021-3](https://doi.org/10.1016/S0304-4203(99)00021-3)
- Wille, J. D., Favier, V., Jourdain, N. C., Kittel, C., Turton, J. V., Agosta, C., et al. (2022). Intense atmospheric rivers can weaken ice shelf stability at the Antarctic Peninsula. *Communications Earth & Environment*, 3(90), 1–14. <https://doi.org/10.1038/s43247-022-00422-9>
- Wolf-Gladrow, D. A., Zeebe, R. E., Klaas, C., Körtzinger, A., & Dickson, A. G. (2007). Total alkalinity: The explicit conservative expression and its application to biogeochemical processes. *Marine Chemistry*, 106(1–2), 287–300. <https://doi.org/10.1016/j.marchem.2007.01.006>
- Zeebe, R. E., & Wolf-Gladrow, D. A. (2001). *CO<sub>2</sub> in seawater: Equilibrium, kinetics, isotopes* (Second pri). Elsevier. [https://doi.org/10.1016/s0924-7963\(02\)00179-3](https://doi.org/10.1016/s0924-7963(02)00179-3)
- Zhou, M., Niler, P. P., Zhu, Y., & Dorland, R. D. (2006). The western boundary current in the Bransfield Strait, Antarctica. *Deep-Sea Research Part I Oceanographic Research Papers*, 53(7), 1244–1252. <https://doi.org/10.1016/j.dsr.2006.04.003>

## References From the Supporting Information

- Dickson, A. G., & Millero, F. J. (1987). A comparison of the equilibrium constants for the dissociation of carbonic acid in seawater media. *Deep-Sea Research, Part A: Oceanographic Research Papers*, 34(10), 1733–1743. [https://doi.org/10.1016/0198-0149\(87\)90021-5](https://doi.org/10.1016/0198-0149(87)90021-5)
- Dotto, T. S., Kerr, R., Mata, M. M., & Garcia, C. A. E. (2021). NAPv1.0: A seasonal hydrographic gridded data set for the northern Antarctic Peninsula. *Earth System Science Data*, 13(2), 671–696. <https://doi.org/10.5281/zenodo.4420006>
- Hansson, I. (1973). A new set of acidity constants for carbonic acid and boric acid in sea water. *Deep-Sea Research and Oceanographic Abstracts*, 20(5), 461–478. [https://doi.org/10.1016/0011-7471\(73\)90100-9](https://doi.org/10.1016/0011-7471(73)90100-9)
- Lueker, T. J., Dickson, A. G., & Keeling, C. D. (2000). Ocean pCO<sub>2</sub> calculated from dissolved inorganic carbon, alkalinity, and equations for K<sub>1</sub> and K<sub>2</sub>: Validation based on laboratory measurements of CO<sub>2</sub> in gas and seawater at equilibrium. *Marine Chemistry*, 70(1–3), 105–119. [https://doi.org/10.1016/S0304-4203\(00\)00022-0](https://doi.org/10.1016/S0304-4203(00)00022-0)
- Mehrbach, C., Culbertson, C. H., Hawley, J. E., & Pytkowicz, R. M. (1973). Measurement of the apparent dissociation constants of carbonic acid in seawater at atmospheric pressure. *Limnology and Oceanography*, 18(6), 897–907. <https://doi.org/10.4319/lo.1973.18.6.0897>
- Millero, F. J., Graham, T. B., Huang, F., Bustos-Serrano, H., & Pierrot, D. (2006). Dissociation constants of carbonic acid in seawater as a function of salinity and temperature. *Marine Chemistry*, 100(1–2), 80–94. <https://doi.org/10.1016/j.marchem.2005.12.001>
- Millero, F. J., Pierrot, D., Lee, K., Wanninkhof, R., Feely, R., Sabine, C. L., et al. (2002). Dissociation constants for carbonic acid determined from field measurements. *Deep-Sea Research Part I Oceanographic Research Papers*, 49(10), 1705–1723. [https://doi.org/10.1016/S0967-0637\(02\)00093-6](https://doi.org/10.1016/S0967-0637(02)00093-6)
- Roy, R. N., Roy, L. N., Vogel, K. M., Porter-Moore, C., Pearson, T., Good, C. E., et al. (1993). The dissociation constants of carbonic acid in seawater at salinities 5 to 45 and temperatures 0 to 45°C. *Marine Chemistry*, 44(2–4), 249–267. [https://doi.org/10.1016/0304-4203\(93\)90207-5](https://doi.org/10.1016/0304-4203(93)90207-5)